GeoScienceWorld
Lithosphere
Volume 2024, Article ID lithosphere_2023_343, 25 pages
https://doi.org/10.2113/2024/lithosphere_2023_343

Lithosphere

Research Article

Controls of Multi-Scale Fractures in Tight Sandstones: A Case Study in the Second Member of Xujiahe Formation in Xinchang Area, Western Sichuan Depression

Junwei Zhao,[1] **Yingtao Yang**,[2] **Gongyang Chen**,[1] **Xiaoli Zheng**,[1] **Senlin Yin**,[1] **and Lei Tian**[3]

[1]*Mud Logging Technology and Engineering Research Institute, Yangtzeu University, Jingzhou, 434020, China*
[2]*Exploration and Development Research Institute, Southwest Oil and Gas Field Company, SINOPEC, Chengdu, 610000, China*
[3]*Oil and Gas Production Capacity Construction Department, Tarim oilfield, CNPC, Korla, 841000, China*

Correspondence should be addressed to Junwei Zhao; zhaojunwei0201@126.com

Received 1 December 2023; Accepted 8 February 2024; Published 1 March 2024

Academic Editor: Yuqi Wu

Different scales of fractures affect the reservoir quality in tight sandstone. There are more studies on macroscopic tectonic fractures but less on bedding fractures and microfractures. The control factors of multi-scale fractures are unclear. In this paper, we analyzed the types and controls of fractures in the second member of the Xinchang region in Western Sichuan. We use core and outcrops observations, imaging logging, scanning energy spectra, and rock slices. Natural fractures can be classified into tectonic, bedding, and microscopic types. The tectonic fractures are mainly low- to medium-angle tensile fractures. The bedding fractures are nearly horizontally distributed along the bedding surface, including parallel, dark mineral interface, and carbonaceous fragments interface bedding fractures. The microfractures develop intra-grain, edge-grain, and inter-grain types. The intra-grain microfractures are inside quartz or feldspar grains, whereas inter-grain types penetrate multiple grains with larger extension lengths. The tectonic fractures are related to the stress, grain size, mineral component, argillaceous content, and lithologic thickness. Parallel bedding fractures are controlled by the coupling of water depth and flow velocity. Bedding fractures at the interface are controlled by rock component. The microfractures are controlled by the length-width axis ratio of the grain, grain element content, and brittleness index. Fractures of different scales form a three-dimensional fracture system that has a substantial impact on the gas production.

1. Introduction

Tight sandstone gas is an unconventional natural resource dominated by low-porosity and low-permeability reservoirs with porosity less than 10% and air permeability less than 1×10^{-3} μm^2 [1–4]. It has been discovered in many basins in China [5–8] and accounts for a relatively large proportion of the gas production, such as in the Ordos, Sichuan, Junggar, and Tarim basins [9–16]. The Xinchang gas field in the Sichuan Basin was first discovered in 1988. The exploration progress was slow owing to the insufficient understanding of geological and fracking processes. After 2,000 years, a few exploration wells were drilled in close to the fracture system, and gas production was increased [17–21]. Exploration showed that the fractures play an important role in controlling the gas production of the Xinchang gas field. However, the distribution of fractures in this zone is complex with different fracture geneses, scales, and occurrences. Nevertheless, there is a lack of the systematic understanding of fractures.

Tectonic fractures in tight sandstones have been extensively studied [22, 23]. The factors affecting them include the stress heterogeneity in different tectonic zones [24–31] and lithologic heterogeneity [32–34]. Sedimentation controls differences in the lithology and layer thickness, and heterogeneity in the mineral composition and structure of reservoirs influence fracture development [35–40]. Bedding fractures are formed by diagenesis and

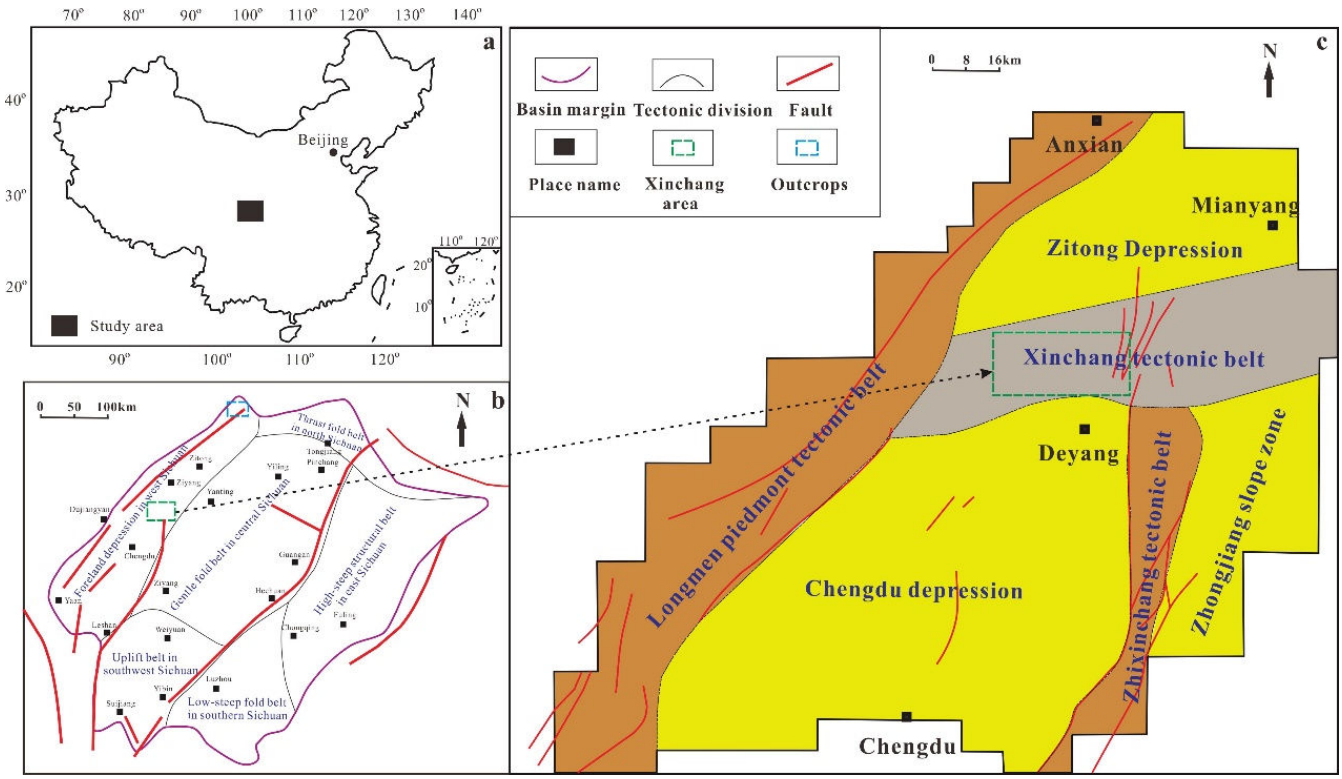

FIGURE 1: Tectonic map of the study area. (a) Boundary sketch of China map; (b) Division of secondary tectonic units in Sichuan Basin; (c) Division of the tectonic units in the Western Sichuan Depression.

tectonics, which are sub-horizontally distributed and can effectively connect different parts of the tight sandstones. They have been extensively studied in shale reservoirs [41–46], but there is less research in tight sandstones, and the types, scale, and controlling factors of bedding fractures are not well studied [47, 48]. Microfractures are important fracture types in tight sandstones that cannot be observed with the naked eye. They have good storage capacity and higher ability to provide seepage channels locally [49, 50]. However, current microfracture studies mainly focus on shale gas reservoirs, and it is believed that quartz, feldspar, organic matter, and carbonate mineral contents are important factors that influence shale microfracture development [51]. The study of them has been limited to their classification and qualitative description [52–56], and a quantitative analysis of the main factors controlling them is lacking. Quantitative characterization of microfracture parameters, such as extension length and fracture aperture, is difficult. Although these parameters can be obtained using rock slices and scanning electron microscopy [57–59], it is more difficult to obtain these parameters for a large number of samples, which also limits the quantitative analysis of microfractures.

In this study, multi-scale fractures of different scales, including tectonic, bedding fractures, and microfractures, were characterized in tight sandstone reservoir in the second member of the Xinchang tectonic zone, and the main factors controlling the fractures at different scales were analyzed. Using core and outcrop data, the classification, quantitative scale, and controlling factors of bedding fractures were discussed. A total of 239 outcrop samples were analyzed by scanning energy spectroscopy and electron microscopy to obtain quantitative parameters, such as elemental components, grain morphology, numbers, extension length, and aperture. The factors affecting the development of micro-fractures are discussed. The relationship between the fracture system and production capacity at different scales was analyzed, which provides a theoretical basis for the exploration and development of the second member of the Xinchang gas field.

2.Geological Background

2.1. Structure. The Western Sichuan depression is located in the western part of the Sichuan Basin, adjacent to the Longmen orogenic belt in the west and bordered by the East Kunlun and Qinling orogenic belts in the north and east, respectively (Figures 1(a) and (b)) [60]. With Longmen Mountain as the boundary, the Western Sichuan Depression can be divided into southern, middle, and northern parts. The Xinchang tectonic zone is located in the middle part of the depression (Figure 1(c)) [61]. It was influenced by multi-phase tectonic movements and formed a northeast-oriented narrow anticline. The two wings of the anticline are characterized by steep south and gentle north [62]. During the Indochina-Yanshan period, a tectonic pattern of lower in the west and higher in the east was formed. During the Late Yanshan-Himalayan period, strong extrusion caused overall uplift of the Xinchang tectonic zone and the western part of the structure was raised up. At the end of the Late

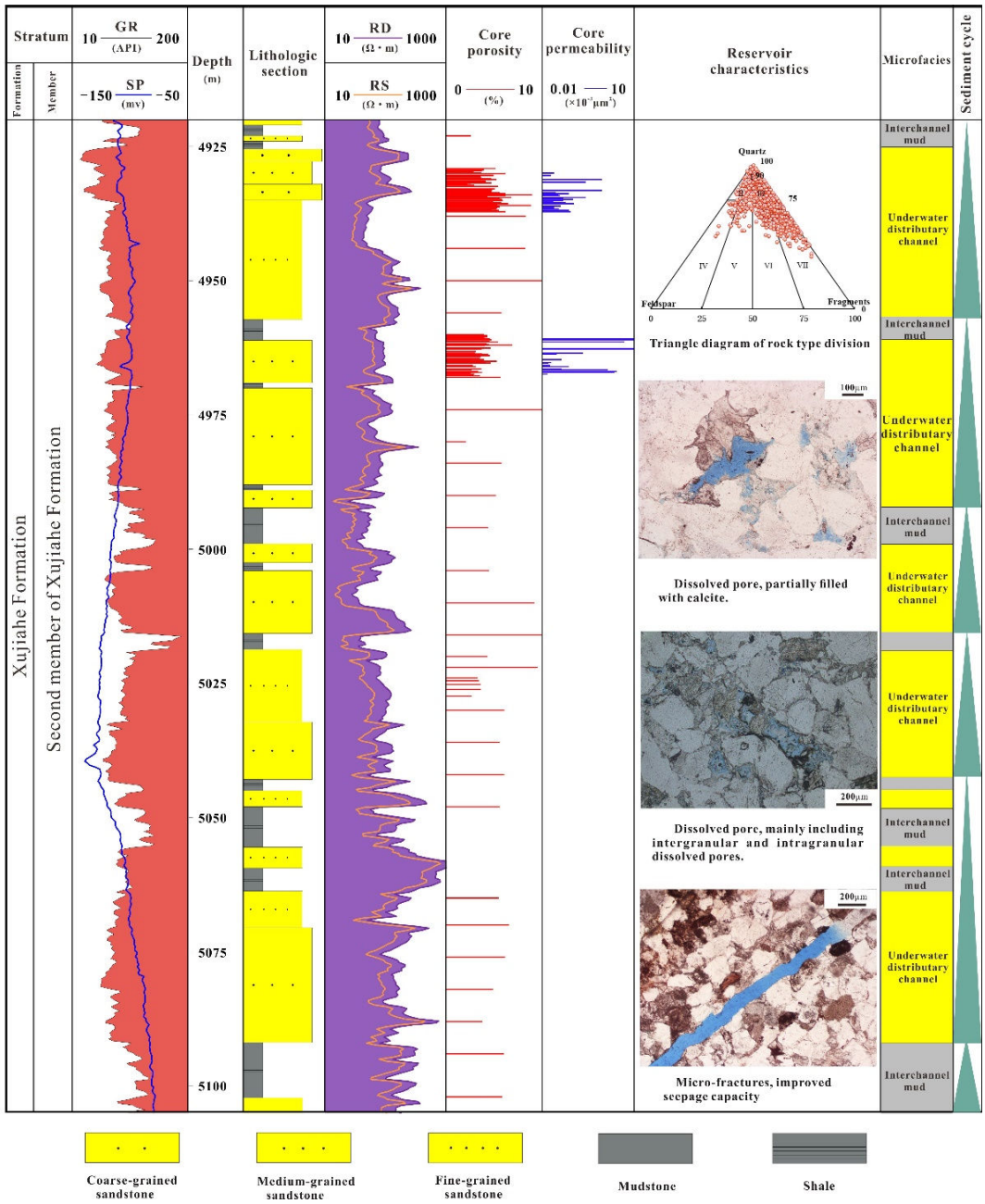

FIGURE 2: Comprehensive characteristics of the reservoir in a typical well of the target layer in the study area.

Jurassic period, natural gas began to accumulate in large quantities, but the reservoir had not yet densified and the natural gas reservoir was formed in the high part of the structure under the effect of buoyancy. After the reservoir was fully densified, the Late Yanshan-Himalayan tectonic adjustment caused an adjustment of the preformed gas reservoir [63, 64].

2.2. Stratigraphy and Reservoirs. The Xinchang tectonic zone has developed a thick Late Triassic-Cretaceous stratigraphy. The stratigraphy includes the Xujiahe Formation of the Upper Triassic, Jurassic, Cretaceous, Tertiary, and Quaternary, and the Xujiahe Formation can be divided into the first to sixth members from bottom to top. The first and third members are thick-layered mudstone deposits [65, 66]. The target layer of this study was the second member, a thick sandstone with thin-layered mudstone (Figure 2).

The study area is dominated by deposits of submerged distributary channels of braided rivers, with small amounts of estuarine bar deposits [67–69]. The burial depth of the reservoir in the second member is approximately 4800–5200 m, and the cumulative thickness of the sand body can be as large as 430 m. The thickness of the sand body in a single channel is approximately 1.5–10 m. Submerged distributary channels of different periods are superimposed,

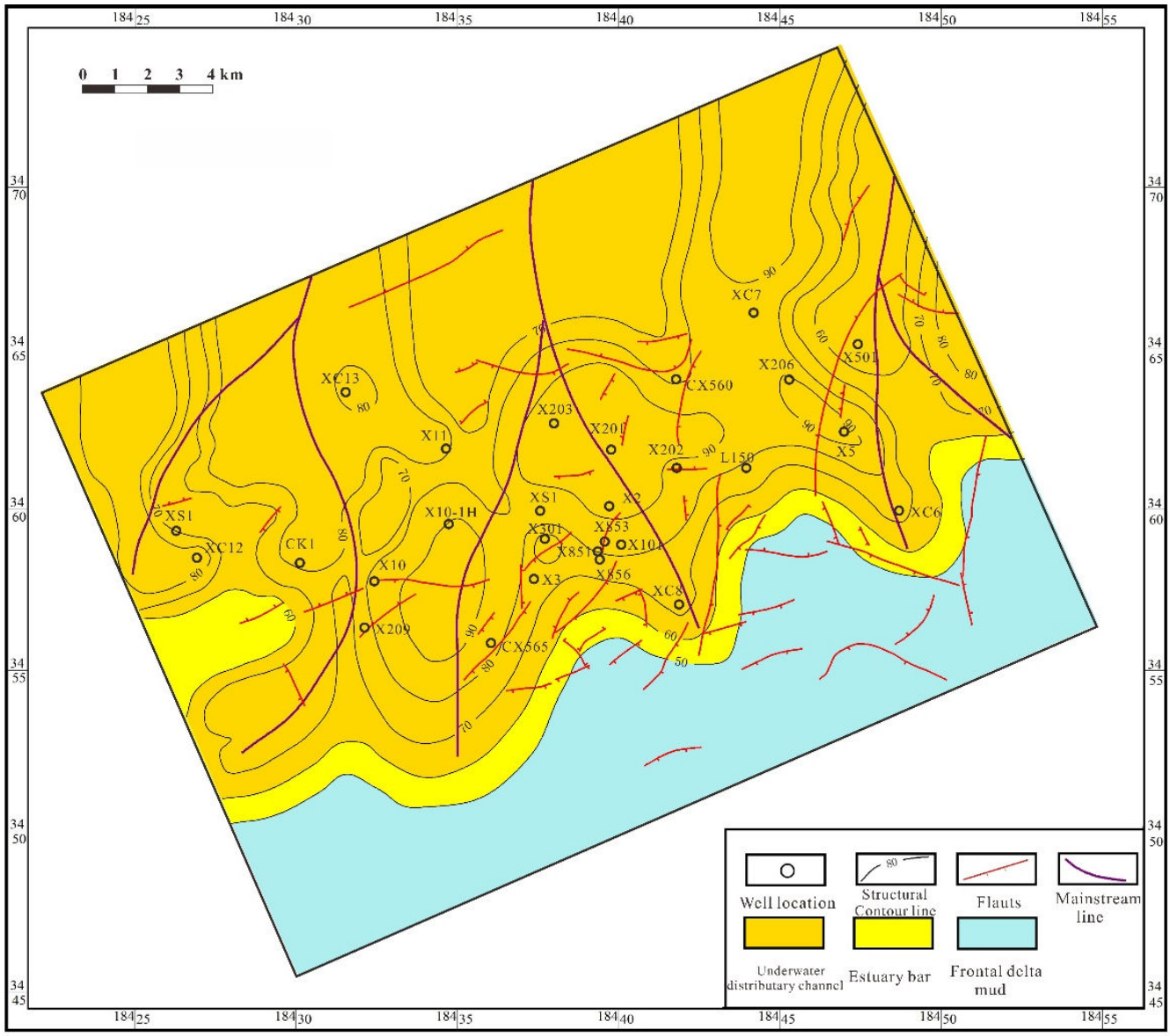

Figure 3: Sedimentary distribution in the middle section of the second member of Xujiahe Formation.

forming a complex sand body in space (Figure 3). The rock type is dominated by lithic and feldspar sandstone, and the grain size is dominated by medium sandstone, with medium sandstone accounting for 67.02% of the total sample, fine sandstone for 21.48%, coarse sandstone for 10.06%, and siltstone for 1.44%. The tight sandstone is strongly diagenetic, with strong reservoir heterogeneity and poor quality, and the pore type is mainly secondary pore with a small amount of primary pore. The average porosity is approximately 3.7%, and the average permeability is less than 0.1×10^{-3} μm^2, which is a typical tight reservoir. The lateral variation in porosity and permeability is large, and the capacity of neighboring wells greatly varies. Affected by multiphase tectonic movement, fractures are more developed, and the complex fracture affects the efficient exploration and development of gas fields [70–73].

3. Samples and Methods

3.1. Samples Preparation. In this study, drilling data of 28 wells, coring data of 17 wells (total 332.4 m), imaging logging data of 17 wells, and outcrop data were used. The number, orientation, and dip angle of fractures were obtained using imaging logs. The tectonic fractures were described using core and imaging data. The bedding fractures were described in the outcrop profiles of Gongnongzhen, which is located at the northern part of the Sichuan Basin. A total of 239 samples were obtained from outcrops using a core sampling instrument.

The imaging logging data of 17 wells were preprocessed, and the depth was corrected using the GR (gamma ray) curve, which was statically and dynamically enhanced, with a uniform color scale for static images and a sliding window

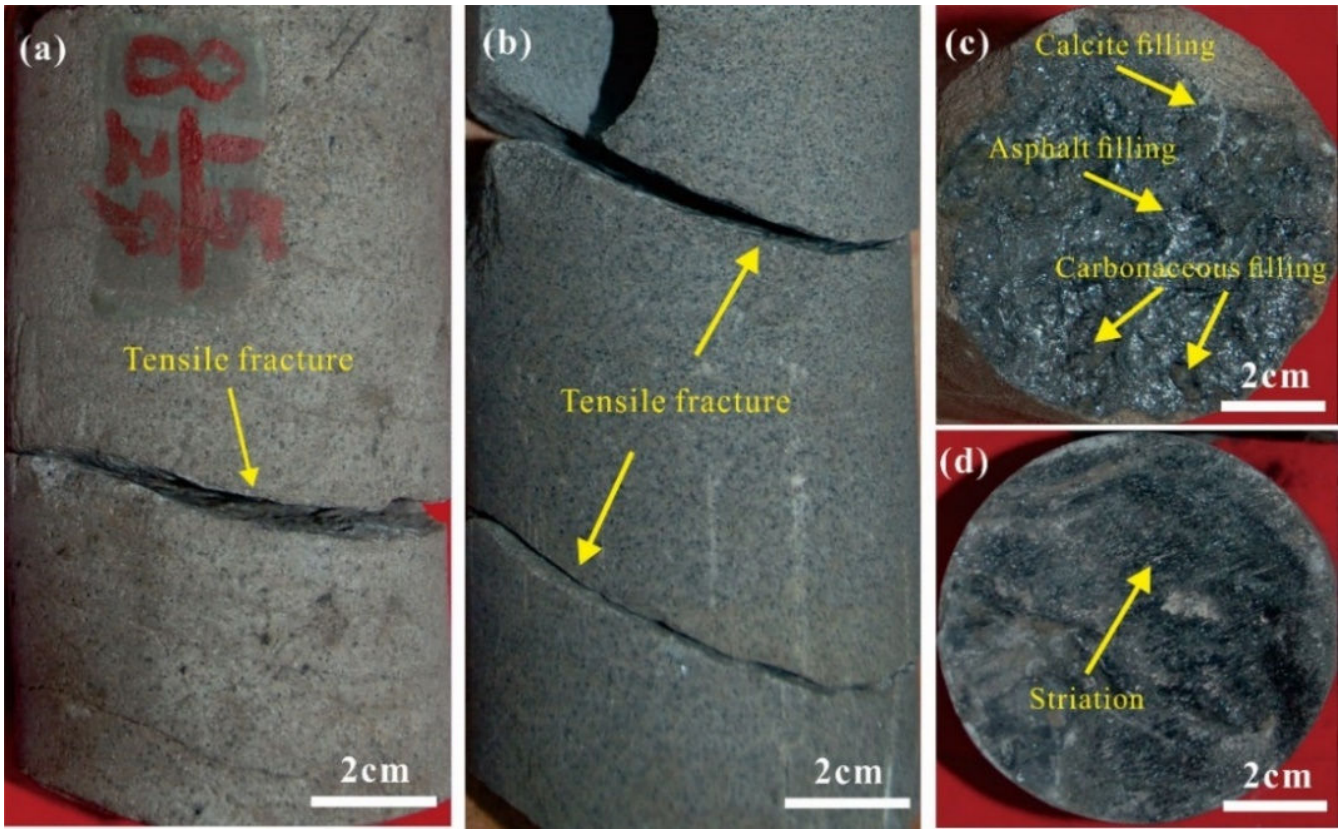

Figure 4: Characteristics of natural tectonic fractures in the second member in cores. (a) Low-angle tensile fracture, unfilled, well X5, 4930–4930.15 m; (b) medium-low angle oblique tensile fracture, unfilled, well X201, 4889.15–4889.3 m; (c) tensile fracture surface, partially filled, mainly filled with asphalt, carbonaceous, and calcite materials, with uneven fracture surface, well XC15, 5156.9 m; (d) Shear fracture surface, partially filled, mainly filled with asphalt and carbonaceous materials, with obvious scuff marks formed by sliding, well XC8, 4975 m.

processing technique for dynamic images. The generation of static and dynamic images can effectively reflect macroscopic and local changes in stratigraphic conductivity. The natural fractures developed in the target layer were interpreted by distinguishing the beddings, muddy strips, and stress-release fractures. The occurrence, effectiveness, and linear density of the tectonic fractures were counted.

Sample elements and microfractures were quantitatively interpreted using X-ray energy chromatography (Energy Dispersive Spectrometer, EDS), and 239 outcrop samples were tested. First, the rock samples were cut and polished to obtain samples of 2 × 0.3 cm in diameter and length, and the samples were put into the center of aluminum foil, and the plastic sealant was placed in the center of the aluminum foil. Then, the samples were pressed with a pressure of 10 MPa for approximately 1 min. Subsequently, the samples were scanned by energy spectrum after plastic sealing, and the mineral grains, pores, and fractures were identified, extracted, and calculated using the scanning results. The parameters, such as elemental content, length-width ratio of grain, total length and number of microfracture, and microfracture aperture, were obtained.

Poro PDP-200 overburden measuring instrument was used to test the porosity and permeability of well samples. Seventy-three samples were tested, and the testing process was fully automated. The diameter and length of 2.54 × 5 cm rock samples were prepared. The samples were washed and dried at 104 °C for 4 hours. Nitrogen was used as the standard test gas. The samples were put into the core holder. The pressure used in the test was automatically controlled by the instrument, and the overburden rock porosity and permeability determination method of the Petroleum Industry Standard SY/T6385-2016 was adopted. The initial pressure applied to the rock sample was 5 MPa, and the pressure was gradually increased as required. The instrument automatically recorded various parameters of the rock sample under different pressure conditions, and the properties were obtained by applying Boyl's and Darc's laws.

The rock cutter and stepless speed control grinder were used to cut and polish the well samples, and 10 pieces of common rock slices were made after gluing. Using the pore-casting instrument, the caster rock slices were made. Rock samples of approximately 25 mm in diameter and 2–4 mm in thickness were cut, and the washed and dried samples were put into the caster, filling under vacuum and pressurized conditions. The main components of the infusion agent were epoxy resin, curing, and dyeing agents. Then, high temperature and pressure curing (temperature approximately 65 °C, pressure approximately 30 MPa) were applied. Subsequently, it was pursued according to the

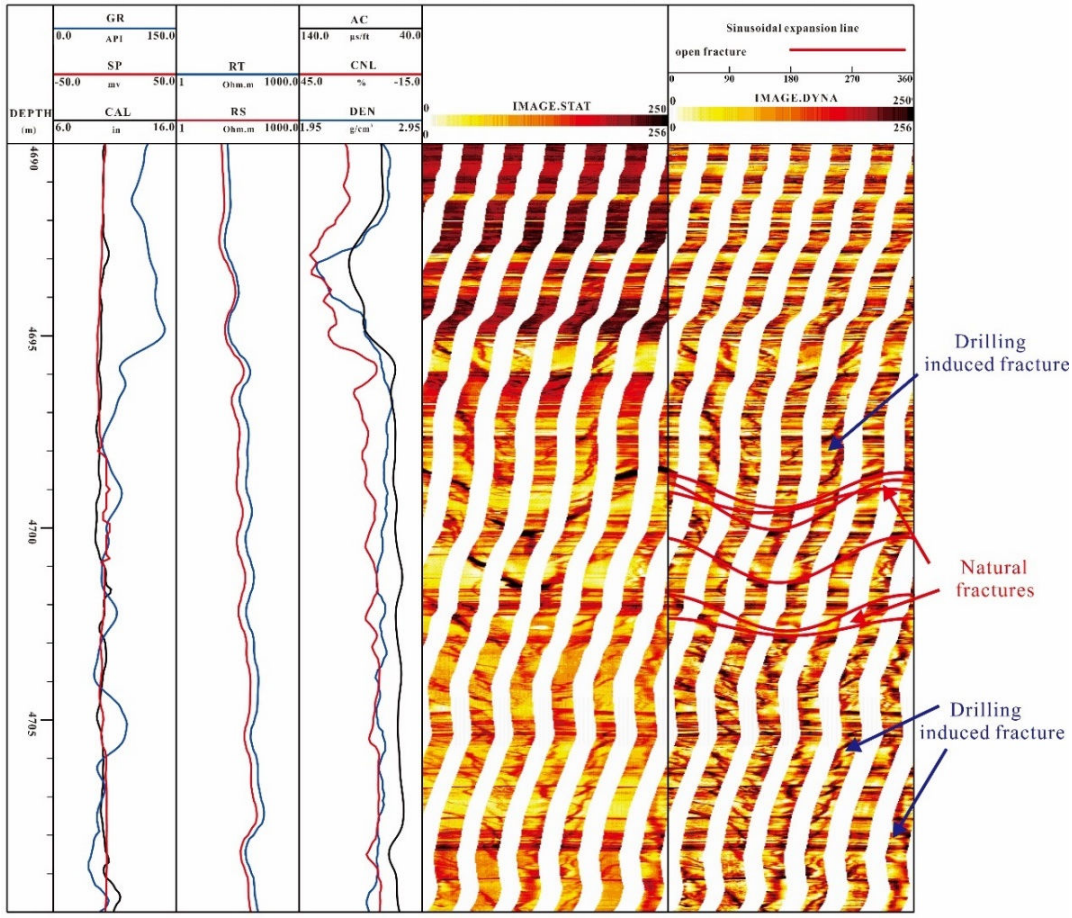

FIGURE 5: Interpretation of tectonic fractures using electrical imaging logs (Well X5) in the second member of Xinchang area.

common rock slice production method, making 63 pieces of casting rock slices. The pore throat structure, porosity, mineral component, and microfracture morphology of the slices were determined in thin sections by counting 300 points per sample using Leica-350. All the above experiments were conducted in the Oil and Gas Resources Exploration and Technology Laboratory, Yangtze University.

3.2. Methods. The fracture linear density was calculated using the results of imaging logging interpretation. It was calculated using equation (1). The brittleness index (BI) of the outcrop samples was calculated by the elemental content using EDS, which was calculated using equation (2).

$$f_L = \frac{n_f}{L} \tag{1}$$

where f_L is the linear density in m^{-1}, n_f is number of fractures in the wellbore direction, and L is the measured length in the wellbore direction.

$$\mathrm{BI} = \mathrm{C_{quartz}}/(\mathrm{C_{quartz}} + \mathrm{C_{carbonate}} + \mathrm{C_{clay}}) \tag{2}$$

BI, brittleness index; C_{quartz}, quartz mineral content, %; $C_{carbonate}$, carbonate mineral content, %; C_{clay}, clay mineral content, %.

4. Results

4.1. Fracture Classification. According to the core and outcrop data, the natural fractures in the second member of the Xinchang area were divided into three categories: tectonic, bedding, and microscopic fractures. Tectonic types include shear and tensile fractures, which are the main macroscopic fractures developed in the layer, mainly large-medium scale fractures. Small-scale bedding fractures are common in the area, with small lateral extension distance, and are formed with the distribution of beddings and rock diagenesis process. Microscopic fractures can be found in the reservoir by scanning energy spectroscopy and rock slices, which are not observable to the naked eye and can be defined as microscale fractures.

4.2. Tectonic Fractures. According to tectonic fracture mechanics [74, 75], the tectonic fractures in the study area can be divided into tensile and shear types, mainly developing tensile fractures (Figures 4(a) and (b)). The surface of the tensile fractures is flat and free of scuff marks (Figure 4(c)), whereas the surface of shear frac-

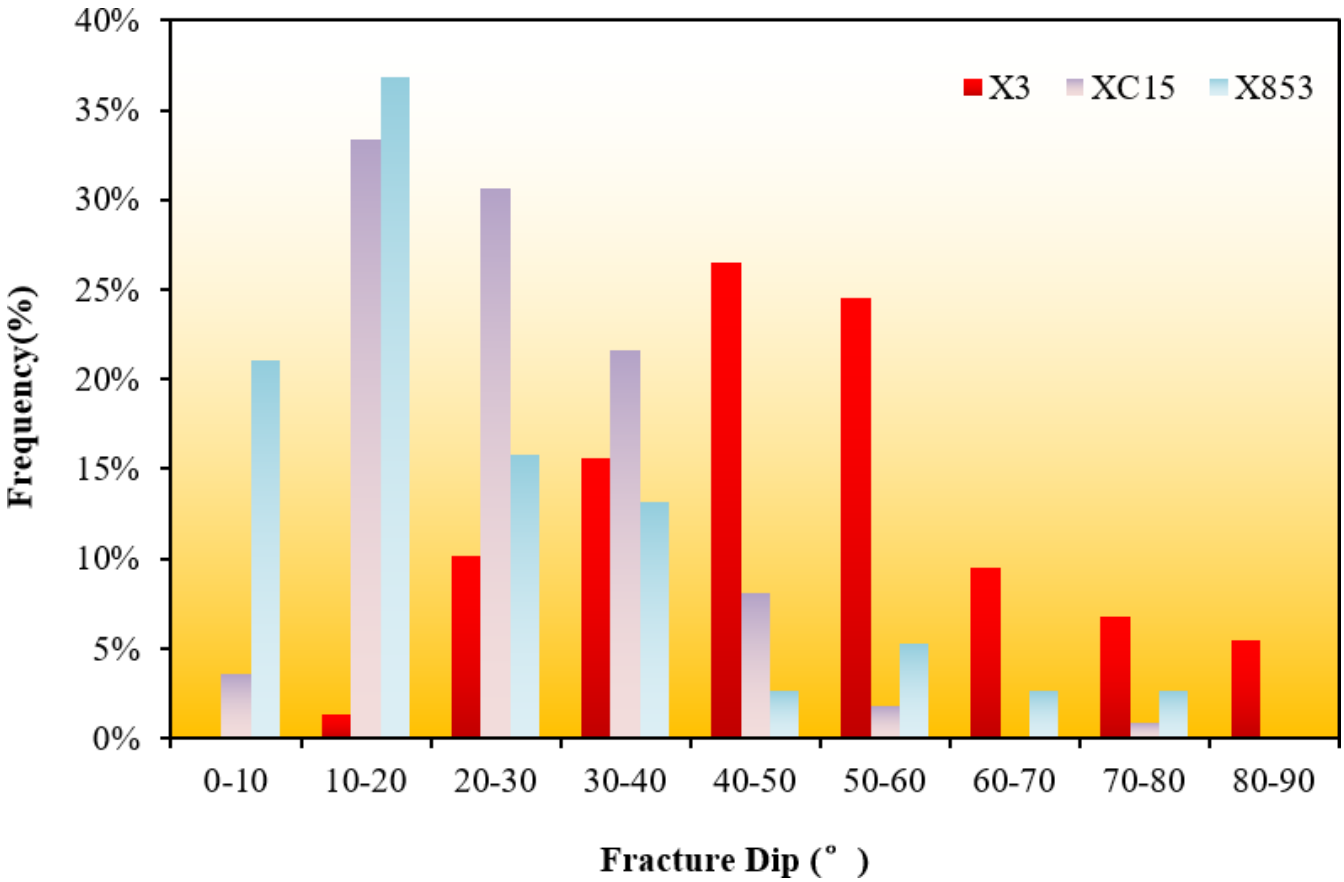

Figure 6: Dip distribution frequency of tectonic fractures in the second member of Xinchang area.

Table 1: Statistics of fracture linear density in the second member of Xinchang area.

Well	Sand group	Number of fractures	Strata thickness (m)	Linear density (m^{-1})
X501	TX_2^4	103	43.85	2.35
X501	TX_2^2	117	99.4	1.18
X501	TX_2^3	112	108.4	1.03
X501	TX_2^5	55	77.95	0.71
X501	TX_2^1	2	54.7	0.04
XC8	TX_2^2	45	73.81	0.61
XC8	TX_2^3	31	85.50	0.36
XC8	TX_2^4	26	73.00	0.36
XC8	TX_2^5	5	59.28	0.08
XC8	TX_2^6	4	79.22	0.05
XC8	TX_2^7	1	71.25	0.01
X209	TX_2^4	24	76.2	0.31
X209	TX_2^2	11	91	0.12
X209	TX_2^3	7	90.5	0.08
X209	TX_2^7	3	51.3	0.06
X209	TX_2^7	3	51.3	0.06
X209	TX_2^5	1	45.16	0.02

tures is visible as scuff marks (Figure 4(d)). Imaging logging data is used to interpret fractures. Drilling-induced fractures and natural fractures are distinguished in the interpretation (Figure 5). The fractures were mainly low- and medium-angle (Figure 6), with low-angle fractures (0, 30°) accounting for 50.94%, medium-angle fractures (30, 60°) accounting for 39.75%, and high-angle fractures (60, 90°) accounting for 9.31%. For example, the percentage of low-angle fractures in well X853 was approximately 73.68%, whereas the percentage of high-angle fractures did not exceed 6% (Figure 6). The fracture-filling status was dominated by unfilled fractures, with the proportion of unfilled fractures being approximately 63.89%, semi-filled being 22.22%, and a small proportion of fractures fully filled with minerals, accounting for approximately 13.89%, with calcite, asphalt, and carbonaceous filling.

The fracture directions of 17 typical wells were analyzed. The results showed that they were mainly distributed in three directions: ESE–WNW to ENE–WSW, NW–SE, and NE–SW. The multi-directional fracture system was formed owing to different tectonic movements. The fractures were heterogeneous, and the linear density of fractures greatly varied from well to well and in a single well (Table 1). For example, the linear density of well X501 was larger, with an average value of up to 1.02 m^{-1}; it was lower in well X209, approximately 0.12 m^{-1}; within the same well, the linear density of fractures also varied in different layers. For

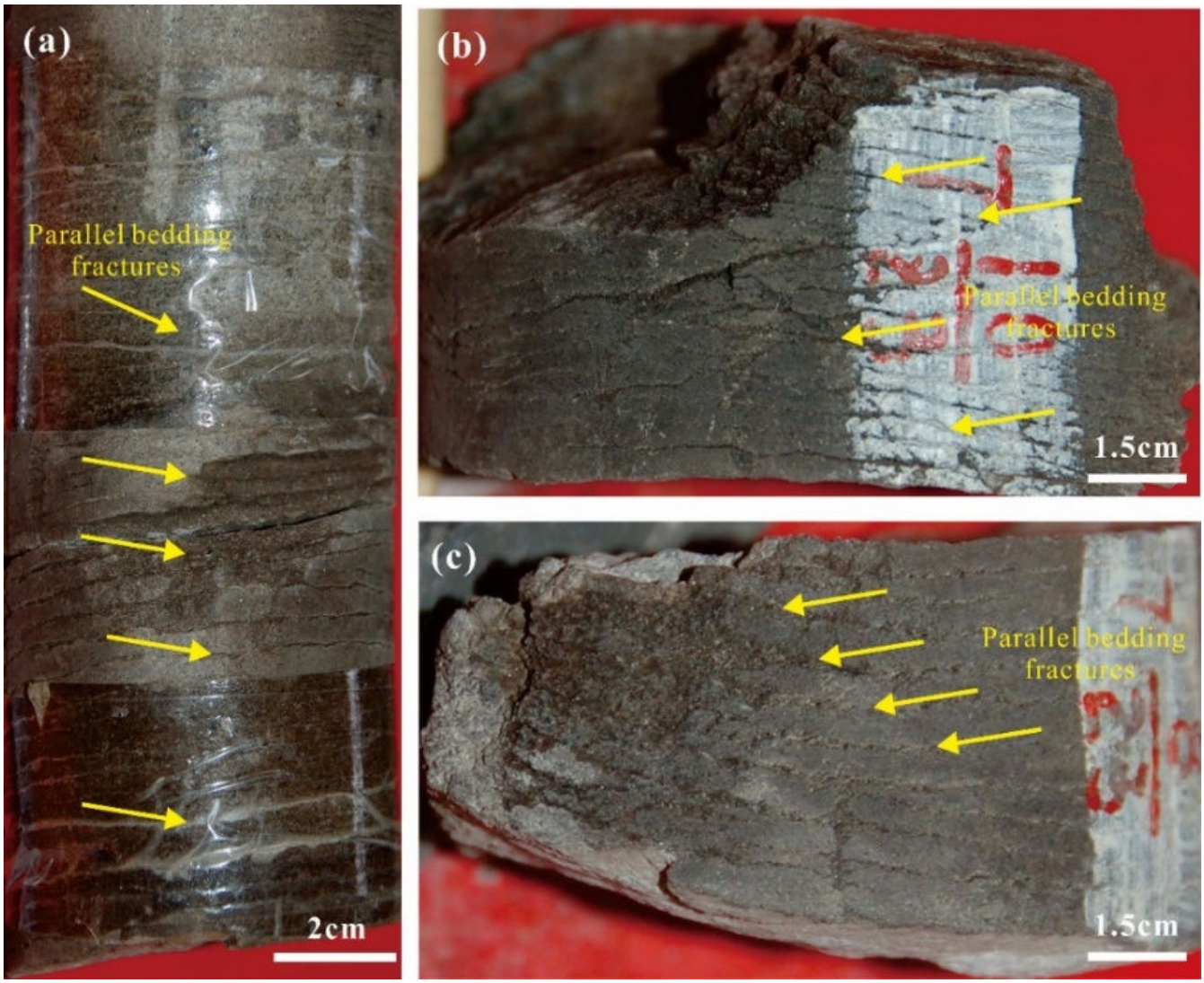

Figure 7: Characteristics of parallel bedding fractures in the core of second member of Xinchang area. (a) Parallel bedding fracture, sub-horizontal distribution, well XC6, 4930–4930.15 m; (b) Parallel bedding fracture, sub-horizontal distribution, well XC6, 4889.15–4889.3 m; (c) Parallel bedding fracture, sub-horizontal distribution, well XC6, 5156.9 m.

example, in well X501, the linear density of the fourth sand group was 2.35 m^{-1}, whereas it was only 0.04 m^{-1} in the first sand group. The tectonic fractures were unevenly distributed in the three-dimensional space, and the fractures were strongly nonhomogeneous.

4.3 Bedding Fractures. More near-horizontal fractures were developed in the tight sandstone in the Xinchang gas field. These fractures were formed along the bedding surface. For example, fractures distributed along different types of beddings were seen in well X5, XC7, and XC6, including cross-bedding and parallel bedding fractures (Figures 7–9) which can be called bedding fractures [76]. The bedding fractures were unevenly distributed in the well, with obvious differences in the degree of development and strong heterogeneity. The core can be divided into the bedding fracture area and the nonbedding fracture area, with the fracture spacing in the well between 0.5 and 15 cm and linear density between 1 and 2.5 cm^{-1} in the bedding fracture developing area. The fracture aperture was larger and more obvious to the naked eye. The fracture surface was uneven, and mica was commonly distributed on the surface. The surface with low mica content was uneven, whereas that with high mica content was straight [48]. The fractures were locally interrupted or bifurcated, and most of them were not filled. They can be divided into the following three categories.

4.3.1. Parallel Bedding Fractures. The bedding type of such fractures is mainly parallel bedding, and the occurrence is nearly horizontal. They are only locally developed in a more limited area, but the linear density of the fractures is larger, locally up to 2.5 cm^{-1}, and the fracture spacing is 0.3–0.5 cm (Figure 7(a)–(c)). The parallel bedding fractures are formed under hydrodynamic conditions of shallow and rapid water flow by mechanically weak interfaces generated by grain

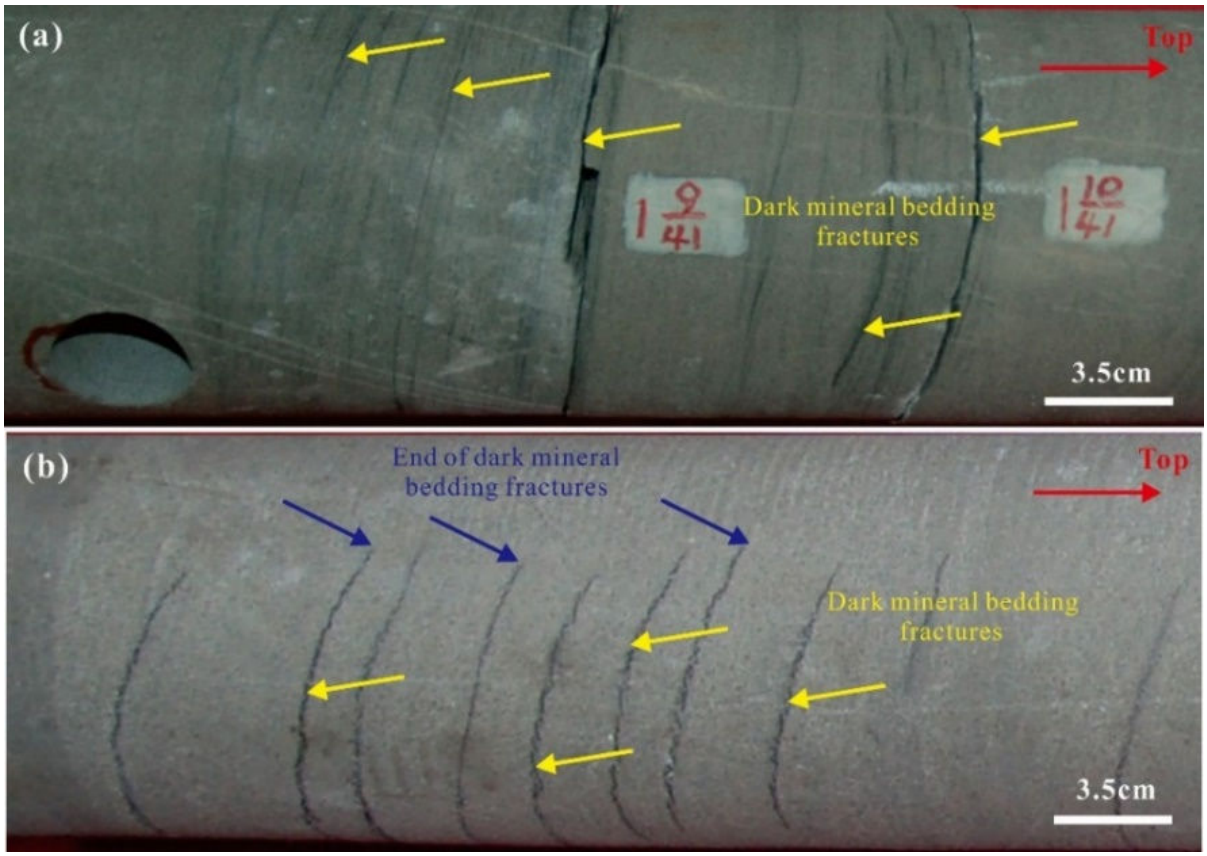

Figure 8: Characteristics of the dark mineral interface fractures in the core of second member of Xinchang area. (a) Dark mineral interface fracture, well X5, 4930–4930.15 m; (b) Dark mineral interface fracture, well X5, 4889.15–4889.3 m.

size differentiation under the action of external tectonic stress [77]. Such fractures are densely locally developed. This can effectively improve the local permeability of the reservoir. For example, the permeability of well XC6 can reach 1.0×10^{-3} μm^2 in the area of parallel bedding fractures.

4.3.2. Dark Mineral Interface Fractures. Such bedding types are mainly cross-bedding beddings, which form dark mineral enrichment owing to hydrodynamic and gravity differentiation [77] and have mechanically weak surfaces at the dark mineral enrichment interface, which can form bedding fractures under favorable stress. The fracture spacing was correlated with the scale of the cross-bedding, and the fracture spacing ranges from 1 to 15 cm (Figures 8(a) and (b)).

4.3.3. Carbonaceous Fragment Interface Fractures. These bedding fractures are formed by hydrodynamic and gravity differentiation of the carbonaceous fragment [77] and form a mechanically weak surface at the interface of the carbonaceous layer. They are formed by tectonic stress after the contraction of rock diagenesis, with a fracture spacing of 0.5–5 cm (Figures 9(a)–(c)).

4.3.4. Scale of Bedding Fractures. From the above classification, it can be seen that bedding fractures are formed by the combination of sedimentary and tectonic stresses. Different beddings form grain size or component differentiation interfaces owing to sedimentary processes and form mechanically weak surfaces during diagenetic process. When the reservoir is subjected to stress, fractures preferentially form at the mechanically weak surfaces. Hence, the bedding fractures generally appear at the surface of sedimentary beddings and are distributed along the beddings. The bedding fractures observed in the cores have very low dip angles and are mostly unfilled. However, they do not always develop at bedding area but are also induced by favorable tectonic stresses.

Because it is difficult to obtain the lateral characteristics of bedding fractures in cores, this study selected the outcrop of the second member of the Gongnongzhen to describe their quantitative characteristics (Table 2). Interpretation of the outcrop shows that the vertical distribution range of parallel bedding fractures is approximately 0.25–0.5 m, the range is small, the spacing of single bedding fracture is 0.5–2 cm, the linear density of them is larger and the lateral extension range is approximately 5–15 m (Figure 10(a)). The vertical distribution range of the dark mineral interface fractures is approximately 3–7 m, the lateral extension range is approximately 3–12 m, and the spacing of the single bedding fracture is 1–15 cm (Figure 10(b)). Carbonaceous interface fractures were not observed in the field, and their vertical distribution is approximately 3–5 m with a single bedding

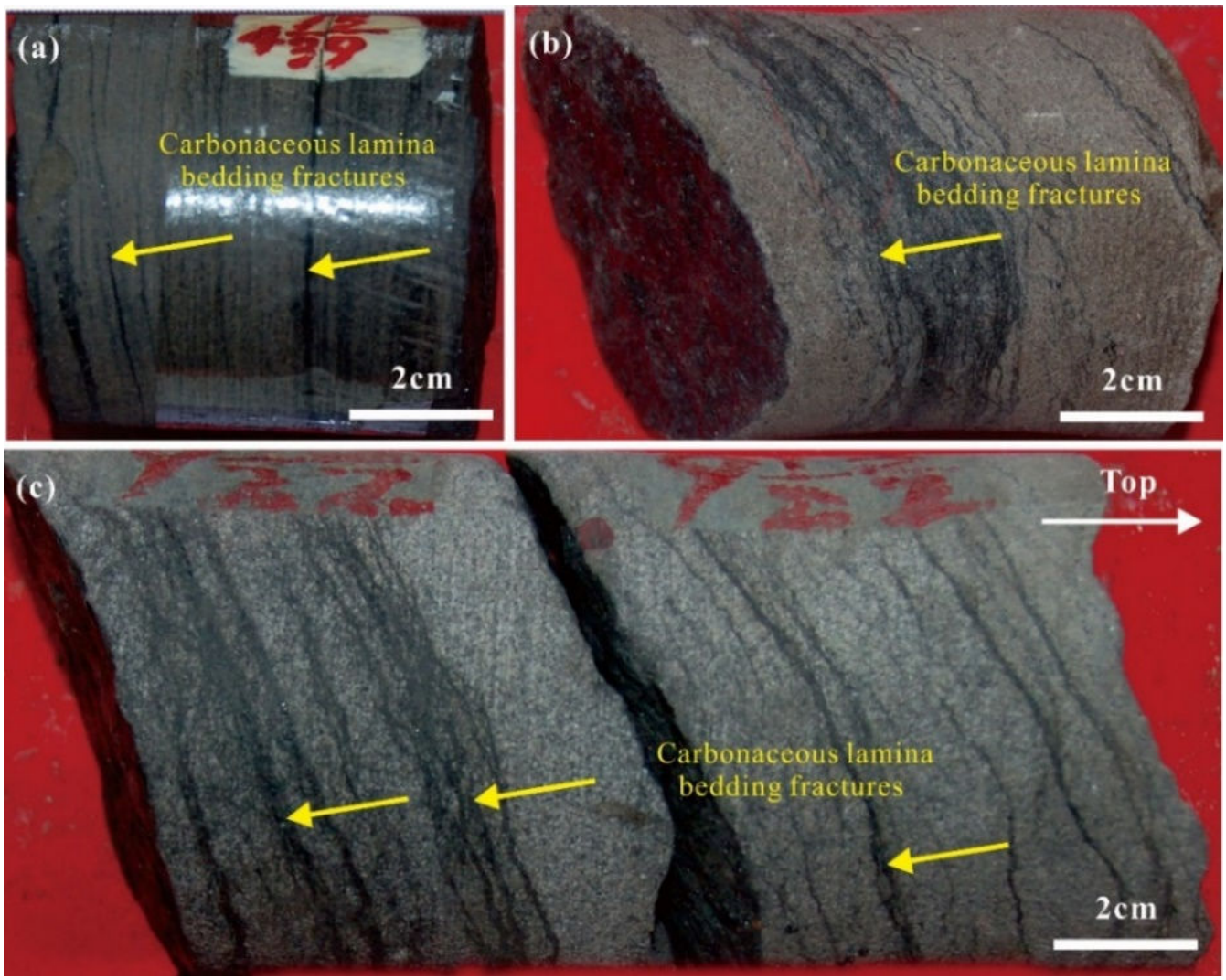

Figure 9: Characteristics of carbonaceous fragment interface fractures in the core of second member of Xinchang area. (a) Carbonaceous interface fracture, well XC15, 4930–4930.15 m; (b) Carbonaceous interface fracture, well XC7, 4889.15–4889.3 m; (c) Carbonaceous interface fracture, well X5, 5156.9 m.

fracture spacing of 1–5 cm according to the core data. However, it should be noted that the bedding fractures in the outcrop differ from that in the subsurface reservoir. The reason why the bedding fractures are more developed in the outcrop is that the mechanically weak surface in the outcrop is more likely to form bedding fractures when the overlying stratigraphic pressure decreases during uplift, whereas the bedding fractures in the subsurface are slightly less developed. Therefore, the quantitative characteristics of the bedding fractures in the outcrop do not represent that of them in subsurface reservoirs but can be used as an important reference in subsurface reservoirs.

4.4. Microfractures. Microfractures are not visible to the naked eye and must be observed under a microscope [78, 79]. EDS tests were performed on rock samples obtained from outcrops and cores in the second member, 239 rock samples were scanned using a combination of energy spectroscopy and electron microscopy. These samples were digitally quantified, and the quantitative parameters of the components, pores, and microfractures were interpreted by automatically extracting this information, which greatly compensated for the shortcomings of the thin-section analysis technique.

The microfractures in the tight sandstone samples are well developed, with the main interval of aperture being 1.46–151.92 μm, average value of aperture being approximately 55.6 μm, main interval of fracture number being 9–799 cm^{-2}, and the main interval of total fracture length being 3.73–93.70 mm cm^{-2}. Combined with the thin-section observations, intergrain microfractures (Figures 11(a) and (b)), marginal (Figures 11(c) and (d)), and intra-grain (Figures 11(e) and (f)) were developed in the study area. The intragrain microfractures are developed inside the quartz or feldspar grains with small extension lengths (Figure 11(e)), approximately 10–400 μm, confined to the interior

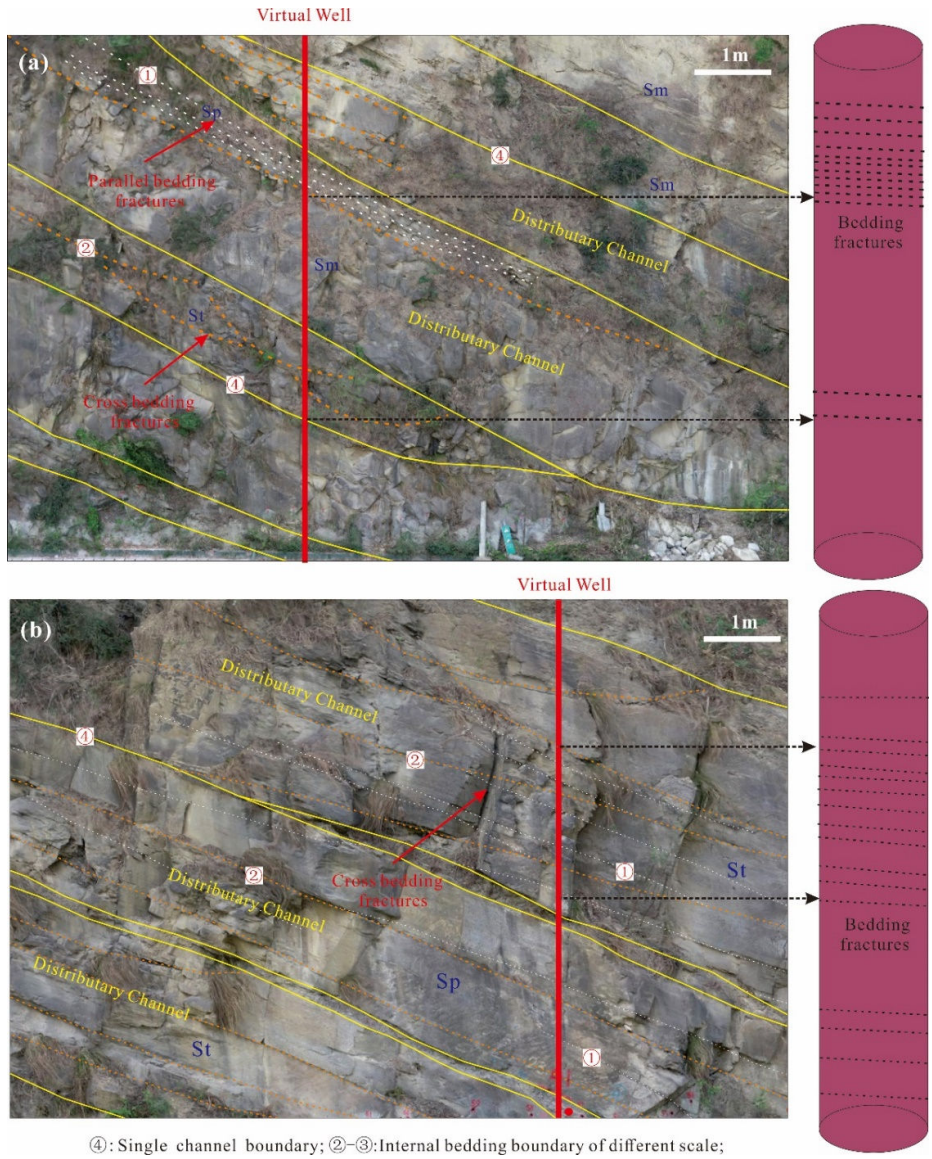

Figure 10: Scale of bedding fractures in the outcrop profile of Gongnongzhen, Western Sichuan.

Table 2: Quantitative relationships of the different types of bedding fractures.

Bedding fracture type	Genesis	Vertical scale	Horizontal scale	Fracture spacing
Parallel bedding interface fractures	Parallel bedding	0.25–0.5 m	5–15 m	0.5–2 cm
Dark mineral interface fractures	Cross-bedding	3–7 m	3–12 m	1–15 cm
Carbonaceous fragment interface fractures	Cross-bedding	1–2 m	/	1–5 cm

of the grains and generally terminating at the edge of the grains, with a small scale in length but a large fracture surface density, mainly on the surface of the quartz or feldspar grains (Figure 11(f)), with small apertures and poor connectivity between the intra-grain microfractures, contributing little to the reservoir permeability. Microfractures at the grain edge have characteristics similar to those of intra-grain types. The intergranular microfractures penetrate multiple grains, and their extension length is not limited by the grains. They extend longer (Figures 11(a) and (f)), often with branching characteristics, and these microfractures are connected with each other, which effectively increase the permeability of the reservoir.

4.5. Different Types of Fractures and Reservoir Properties. Natural fractures provide important reservoir space and seepage channels for tight sandstone reservoirs,

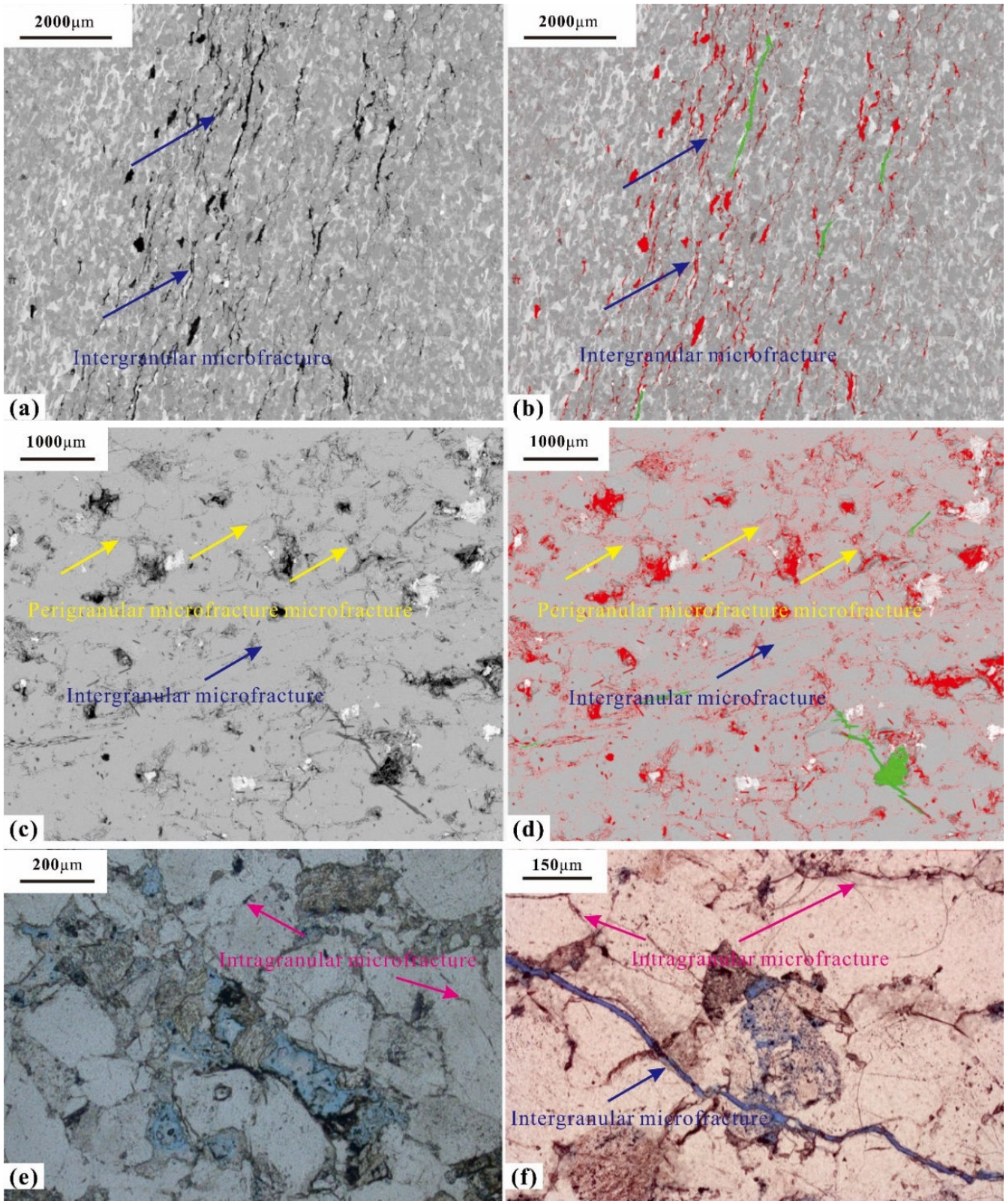

FIGURE 11: Microfracture characteristics of outcrop and well core samples in EDS and rock slice. (a) intergranular microfracture, EDS grayscale map, sample 65 of Gongnongzhen profile, porosity is 5.69%; (b) intergranular microfracture, EDS pore facture interpretation map, sample 65 of Gongnongzhen profile, porosity is 5.69%; (c) intergranular and edge-grain microfracture, EDS grayscale map, well X201, 4916.06 m; (d) intergranular and edge-grain microfracture, EDS pore facture interpretation map, well X201, 4916.06 m; (e) intragranular microfracture, rock slice, well X201, 4820.6 m; (*f*)) intragranular microfracture, rock cast thin section, well XC8, 4971.54 m.

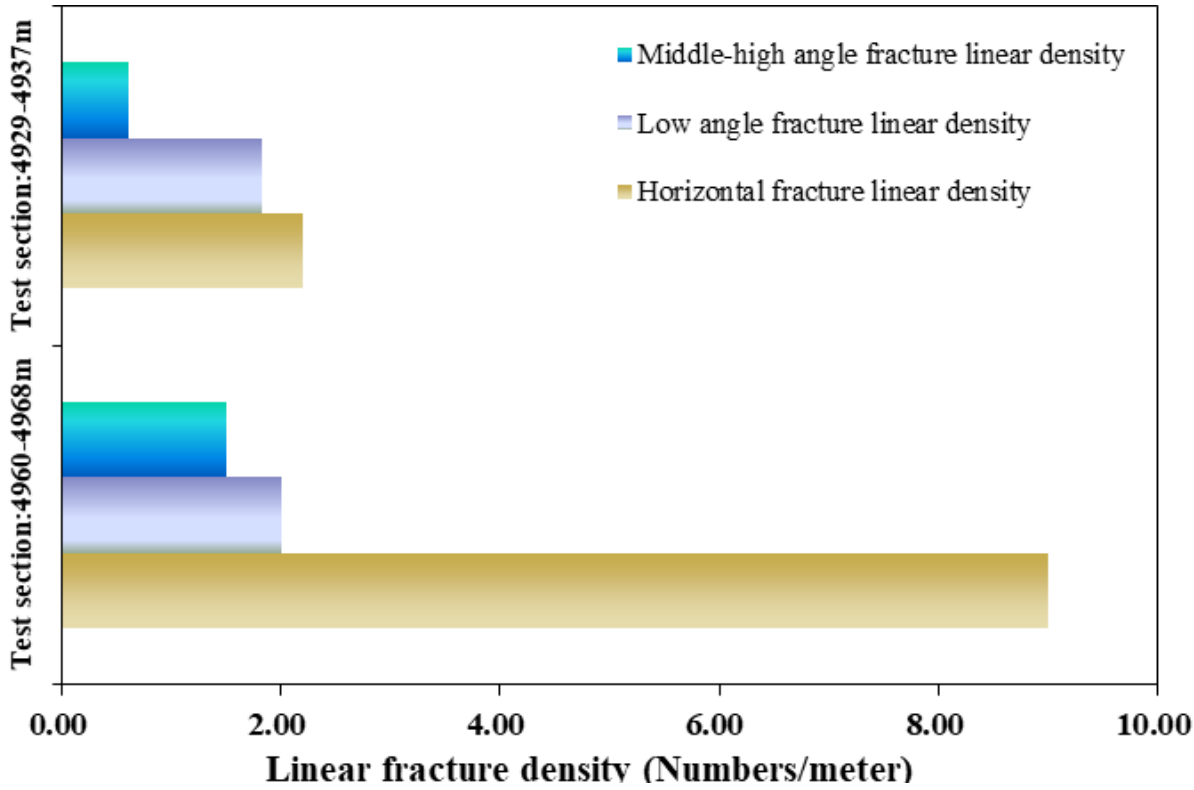

Figure 12: Distribution of fracture linear density in well X5 (4929–4937 and 4960–4968 m).

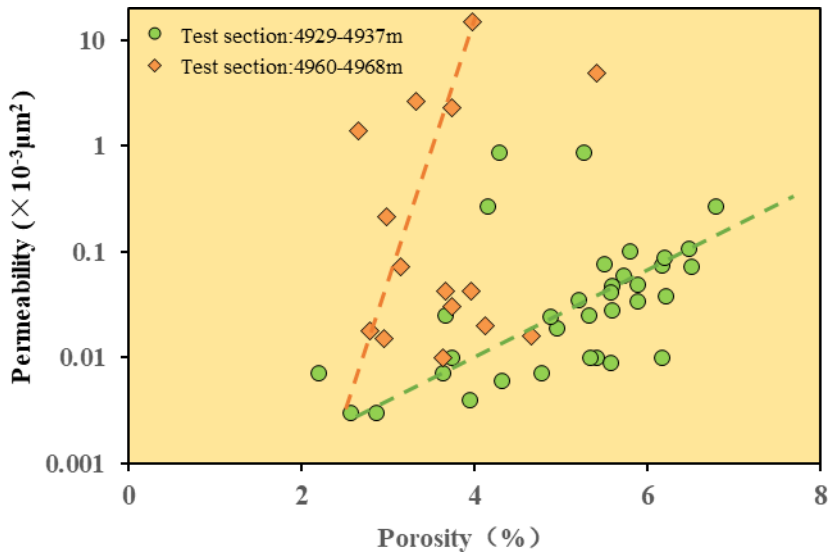

Figure 13: Pore-permeability relationship between small-scale bedding facture developed and undeveloped layers of the reservoir (well X5).

and these types of fractures contribute differently to the reservoir properties. Large- to medium-scale fractures increase reservoir properties, connect small-scale bedding fractures with micro-scale fractures, form a fracture network system, and increase reservoir percolation capacity [80]. Large- and medium-scale fractures can improve the reservoir permeability, which has been analyzed further. The permeability of reservoirs with small-scale bedding fractures substantially increases, but the bedding fractures have limited lateral extension and are vertically independent of each other. Therefore, they can only improve the permeability of local reservoirs. For example, the well X5 does not develop near-horizontal bedding fractures in 4929–4937 m but develops many near-horizontal bedding fractures in 4960–4968 m (Figure 12). The average porosity of the small-scale bedding fracture-developed section is approximately 3.95%, and the permeability interval is 0.01–33.24 × 10^{-3} μm^2, with an

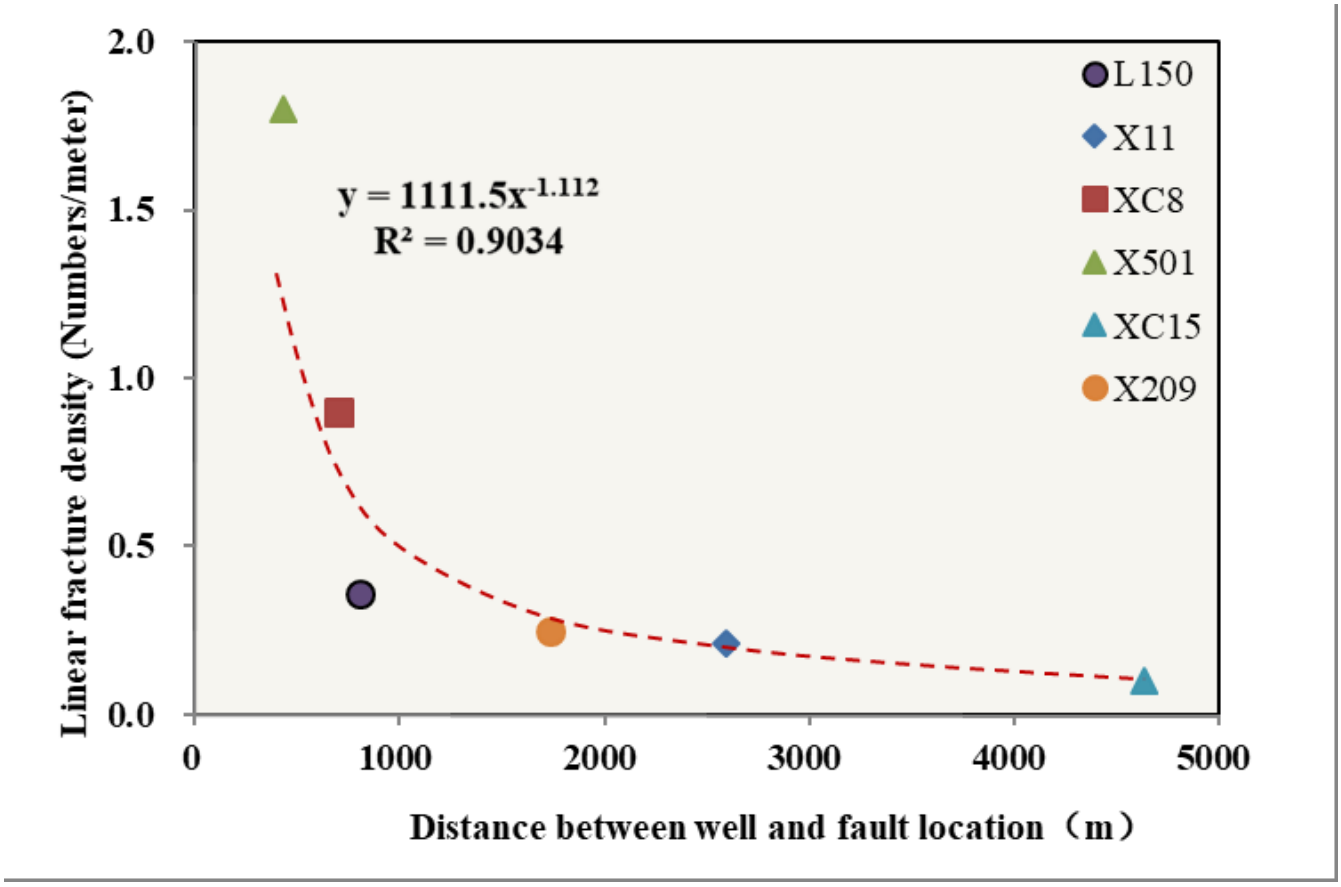

Figure 14: Relationship between fracture linear density and distance from fracture.

average value of 9.35 × 10^{-3} μm² (Figure 13). The average porosity of the section with undeveloped bedding fractures is approximately 4.9%, and the permeability interval is 0.005–0.866 × 10^{-3} μm², with an average value of 0.10 × 10^{-3} μm² (Figure 13). In the microfracture-developed thin slice, the average porosity is approximately 4.57%, and the average permeability is 3.56 × 10^{-3} μm². In the microfracture-undeveloped thin slice, the average porosity is approximately 3.85%, and the average permeability is 0.08 × 10^{-3} μm². The permeability substantially increases in the microfracture-developed area.

5. Discussion

5.1. Main Controlling Factors of Fractures

5.1.1. Factors Controlling Tectonic fractures. The main factors controlling the tectonic fractures have been extensively studied [81, 82]. These fractures in the second member of the Xinchang tectonic zone are controlled by several factors. The tectonic stress is the primary factor and is also closely related to the lithology, stratum thickness, and mechanics layer.

Tectonic action leads to the formation of tectonic fractures [80]. The tectonic stress difference controls the development of these fractures. These fractures in the reservoir show that the closer to the large fault, the more developed the tectonic fractures (Figure 14). For example, the average fracture linear density is 0.21 m^{-1} in well X11, which is approximately 2600 m away from the large fault, and it is 1.83 m^{-1} in well X501, which is approximately 400 m away from the large fault. The better gas-producing wells in the study area are generally located near the main fault or the axis of small folds. Fault activity causes the fracture zone to be subjected to an obvious stress concentration phenomenon, and the fractures are more developed near the zone. Therefore, the differences in tectonic zones and the distance from the main fault control the tectonic stresses on the reservoir, which in turn affect the tectonic fracture linear density.

Lithological differences affect the fracture development in the reservoir, and the lithology influences fractures through grain size, mineral component, argillaceous, and calcareous cement content. The statistical results of fracture linear density for different lithologies show a relationship between grain size and average linear density (Figure 15). For example, the linear density of medium sandstone in well X501 is the larger, up to 1.83 m^{-1}, whereas that of fine sandstone is smaller. The grain components of reservoirs are various, and their elastic moduli and Poisson's ratios are substantially different, leading to form different fractures under the same stress. For example, the linear density of the quartz sandstone in well X201 is larger, up to 0.83 m^{-1}, and that of the lithic sandstone is smaller, approximately 0.1 m^{-1}.

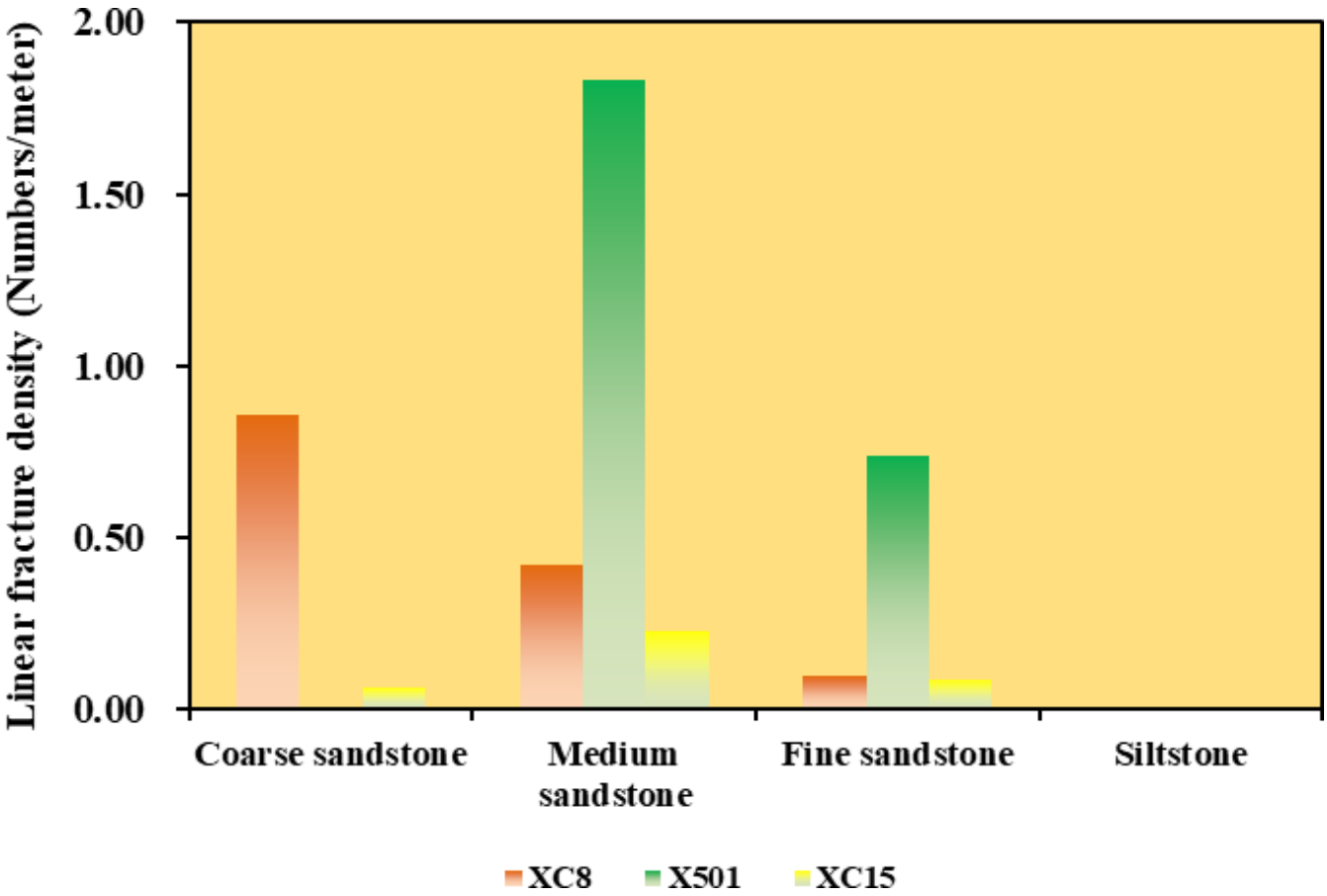

Figure 15: Relationship between fracture linear density and grain size.

A higher content of brittle minerals is favorable for tectonic fracture development. The favorable petrographic type for these fractures is quartz sandstone. The argillaceous content also influences the fractures. To eliminate the influence of grain size and mineral components, layers with similar grain size and components in well X501 were selected to discuss the effect of argillaceous content on tectonic fractures. It can be seen that the argillaceous content and tectonic fracture linear density are negatively correlated (Figure 16). When the argillaceous content is greater than 15%, the linear density is very low.

Rock mechanics layers are lithologic layers with the same or similar rock mechanical properties. The layers generally terminate at the mudstone interface. Tectonic fractures are usually developed inside rock mechanics layers, and very few fractures can cross mudstone layers [74]. It can be found that there is a substantial relationship between the thickness of the rock layers and the fracture linear density. To eliminate the effect of lithology, the fracture linear density of the medium sandstone was analyzed. It is clear from the graphs that it shows a certain correlation (Figure 17), where the linear density decreases with increasing layer thickness, and a threshold thickness exists in each well, above which the fracture linear density does not change much as the layer thickness increases. Less than this threshold, the fracture linear density becomes larger in a certain range as the thickness decreases.

5.1.2. Factors Controlling Bedding Fractures. The bedding fractures are related to various factors. The formation of them can be mainly attributed to sedimentation and diagenesis, whereas tectonics is the triggering factor [48]. For these fractures, sediments were subjected to continuous increases in the overlying stratigraphic pressure during diagenesis, and sediment grains at different types of bedding interfaces underwent differential compaction and cementation [48], such as the interfaces of dark- and light-colored mineral. The two types of mineral compaction pressure are not consistent, and the fractures are distributed along the bedding interface in the process of diagenesis. For similar reasons, the parallel beddings are composed of layers with different grain sizes. There are differences in grain sizes between the layers. Moreover, there are differences in the compaction process of the layers with different grain sizes during diagenesis, with coarse grains having strong compaction resistance and fine grains having weak compaction resistance. Compaction occurs at the interface of the fine grain layers, forming mechanically weak surfaces and parallel bedding fractures, developing stripping lineation structure. These fractures formed during diagenesis are subjected to tectonic stress. The scales of the fractures are modified to some extent. Therefore, the bedding fractures are controlled by endogenous factors. Parallel-bedding fractures are mainly controlled by parallel bedding, and the bedding fractures at the interface of

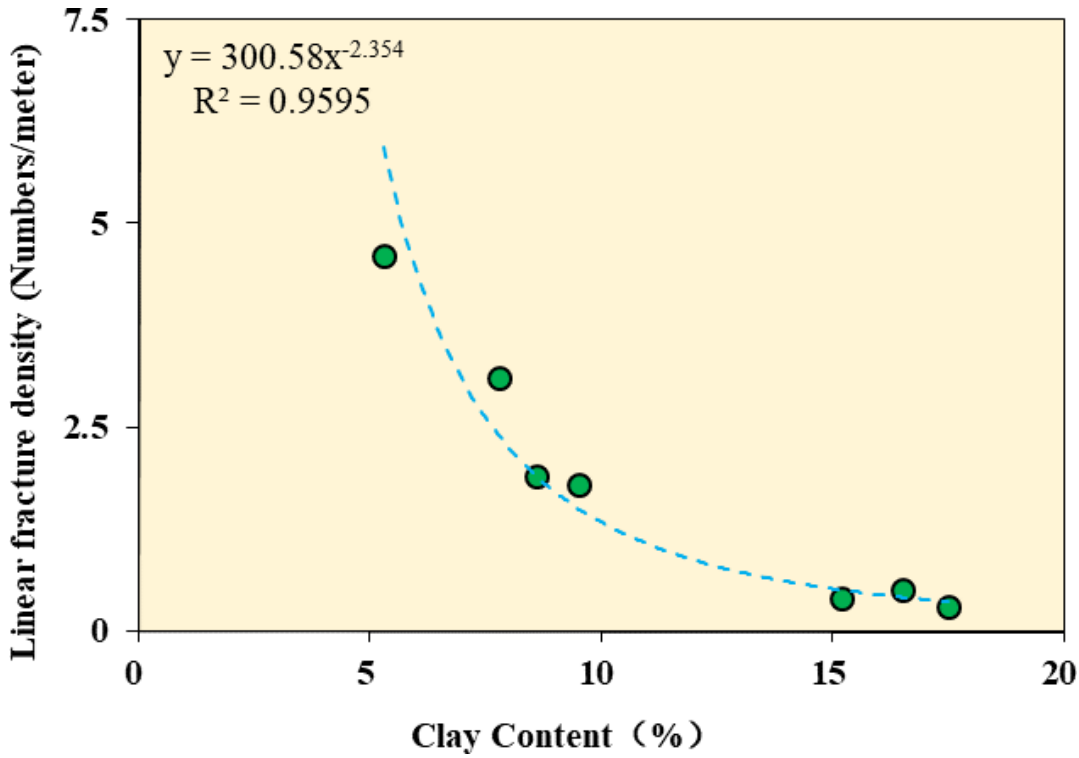

Figure 16: Relationship between fracture linear density and argillaceous content.

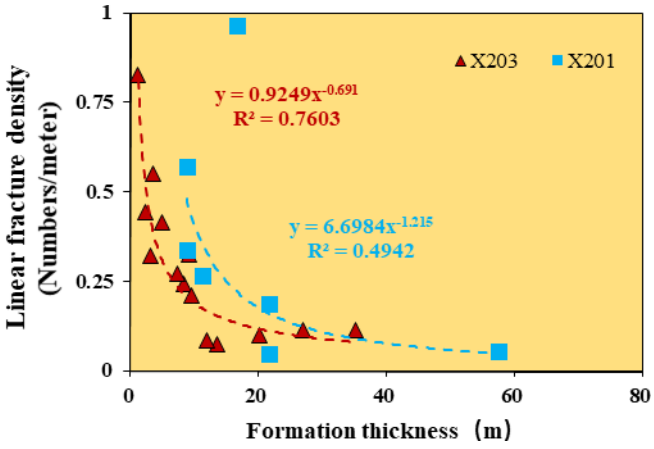

Figure 17: Relationship between fracture linear density and lithology thickness.

dark minerals and carbonaceous layers are controlled by differences in rock components.

The thickness of the submerged distributary channel in the second member is large, with an average thickness of 2–10 m. The channel water depth is large during the deposition period, with a strong hydrodynamic force and sufficient supply of sediment sources. The reservoir only develops parallel bedding in some wells. The formation of these beddings is influenced by the Froude Number, as shown in the following equation:

$Fr=V/\sqrt{h \cdot g}$, where v is the average flow velocity, m/s and h is the water depth, m.

When Fr < 1, the water flow velocity is small, which represents the characteristics of deep water and slow flow. When Fr = 1, the water flow is critical flow. When Fr > 1, the water flow velocity is large, which represents the characteristics of shallow water and rapid flow. The Fr index reflects the change in the reservoir bedding type, the hydrodynamic condition of parallel bedding is an Fr index close to 1 when the water depth is smaller, and the flow velocity is larger. Observation of the cores shows that the parallel beddings are more developed at the top of the single-phase subchannel. In the late stage of deposition, the channel is continuously filled and the channel depth decreases, whereas the hydrodynamic force is still strong at this time. The coupling between the flow velocity and depth of the channel is formed, which makes it easy to form parallel beddings and mechanically weak interfaces with different grain sizes, and parallel bedding fractures develop along the interfaces.

The bedding fractures at the interface of the dark minerals and the carbonaceous texture are owing to the existence of different components. Well data with bedding fractures developed and undeveloped were selected for analysis, and the differences in the quartz, feldspar, and rock fragment contents were compared. It should be noted that rock fragments are not equivalent to dark minerals, but the higher content of rock fragment reflects the low maturity of rock components, whereas the content of dark minerals should be higher. The content of rock fragment can be used to indicate the content of dark minerals. Figure 18 shows that the quartz and feldspar contents are generally less than 75% in the bedding fracture developing

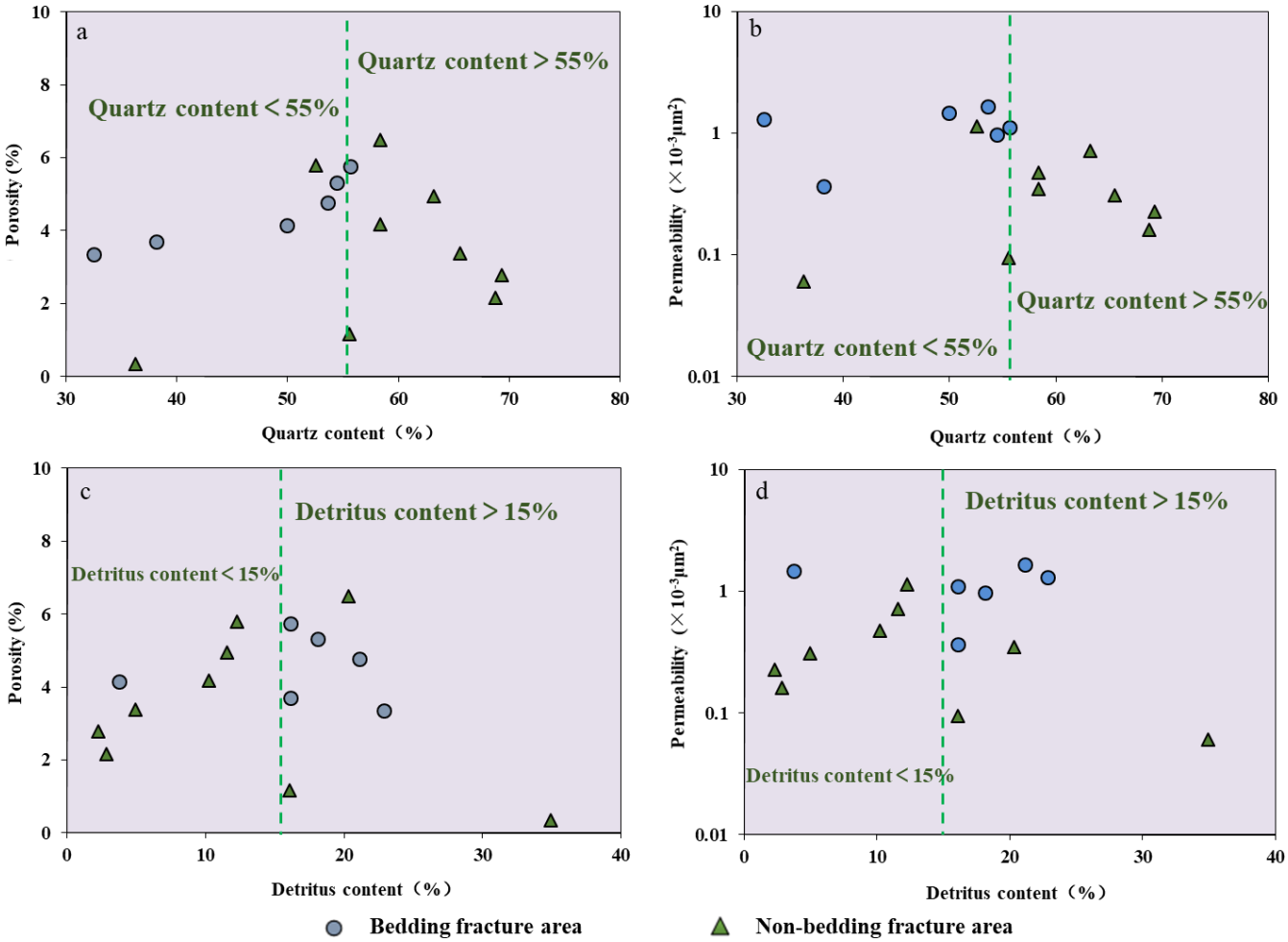

FIGURE 18: Influence of rock components on the development of bedding fractures at the interface of dark minerals.

layers, and the rock fragment content is generally more than 25%. The high percentage of rock fragment content represents the high content of dark minerals, which are prone to form a dark mineral-rich divergent interface under the effect of gravitational divergence during the deposition process, generating a mechanically weak surface. When the rock fragment content is too low, the sediment has a low content of dark minerals, which tends to form a homogeneous sediment of quartz and feldspar and is not conducive to the formation of a gravity-divergent interface (Figures 18(a)–(d)). The bedding fractures at the carbonaceous fragment interface are also owing to the carbonaceous debris enrichment. The enrichment of carbonaceous debris is related to the sediment supply. The above analysis shows that for tight sandstones with lower compositional maturity, a higher rock fragment content is favorable for the formation of bedding fractures.

5.1.3. Factors Controlling Microfractures. The microfractures are related to a variety of factors. Similar to macrofractures, the higher the tectonic stress to which the reservoir is subjected, the more microfractures will develop. They are also controlled by the intrinsic factors of the tight reservoir, including the grain size, grain component, interstitial material content, and the inter-grain contact relationship. To eliminate the influence of tectonic stress on microfractures, samples from the outcrop were selected for discussion. The outcrop is subjected to similar tectonic stress, which can effectively explain the influence of endogenous reservoir factors on microfractures.

5.1.3.1. Aspect Ratio of Grain. The analysis of the quantitative parameters of microfractures in 239 samples from the outcrop shows that the total length, number, and aperture of microfractures developed per unit area are controlled by the shape of the grains (Figure 19), mainly the ratio of the long to short axes of the grains (hereinafter referred to as the grain aspect ratio). The ratio has a substantial negative relationship with the total length and aperture of microfractures. The larger the grain aspect ratio, the smaller the total length of the microfractures per unit area (Figure 19(a)) and the smaller the aperture (Figure 19(c)), which has no substantial relationship with the total number (Figure 19(e)). If the grain aspect ratio is distributed between 2.7 and 3.5, the corresponding microfracture length and aperture are 0–60 mm/cm^{-2} and 1–7 μm, respectively. When the grain aspect ratio is distributed between 1 and 2, the above parameters are 30–120 mm/cm^{-2} and 70–150 μm,

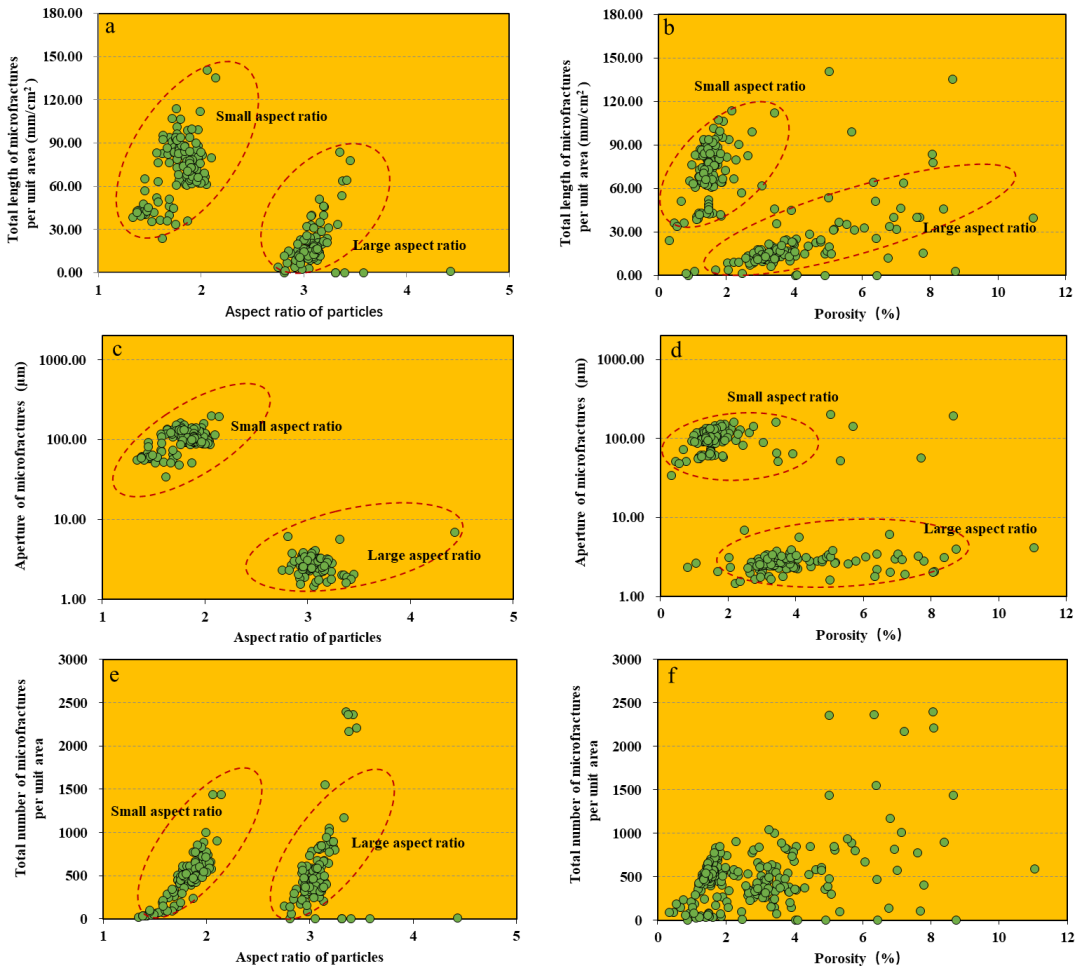

FIGURE 19: Relationship between grain aspect ratio, porosity and total length, aperture, and total number of microfractures.

respectively. The ratio of the grains and the porosity has a certain relationship (Figure 19), the larger the ratio, the greater the porosity. Thus, there is an indirect correlation between the porosity and the total length and aperture of the microfractures (Figures 19(b), (d) and (f)). The ratio is correlated with the grain morphology. The above relationship can be explained by the fact that the closer the grain morphology to a spherical shape, the more favorable the development of microfractures, the area of mutual contact between spherical grains is small, and the tectonic stress per unit area is larger, which is conducive to the forming of microfractures. On the contrary, the larger the ratio, the larger the area of mutual contact between grains after strong compaction, and the tectonic stress per unit area is smaller, which limits the forming of microfractures. The causes of grain morphology are complex and related to the weathering of parent rock and sediment transport processes.

5.1.3.2. Element content. Microfractures are also influenced by the content of the grain components, which are closely related to the elements. The correlation between the element content and microfractures was analyzed based on the results interpreted by EDS. Microfractures are strongly influenced by the silicon (Si), calcium (Ca), and aluminum (Al) contents (Figure 20). Si and Ca elements are the brittle elements, but there is a difference in the control of the microfracture morphology: the higher the Si element content, the more microfractures developed (Figure 20(a)). Quartz grains have a high content of silicon, and a large number of microfractures developed inside the quartz grains. No substantial relationship was detected between the Si element content and the total length of microfractures (Figure 20(b)), indicating that a high Si content is favorable for the microfractures inside the grains, and the number of fractures is large, but the length is small. The Ca content is negatively correlated with the total number of microfractures (Figure 20(c)) and positively correlated with the total length (Figure 20(d)). A set of calcareous sandstone with high Ca content is developed in the upper part of the outcrop, and the average Ca content can reach 30%. The microfractures inside the calcareous sandstone are characterized by a small total number and a large total length of fractures, indicating that the high content of Ca elements is conducive to the forming of inter-granular microfractures, and the number of microfractures developed is small, but the length is large. The Al content is negatively correlated with the formation of microfractures,

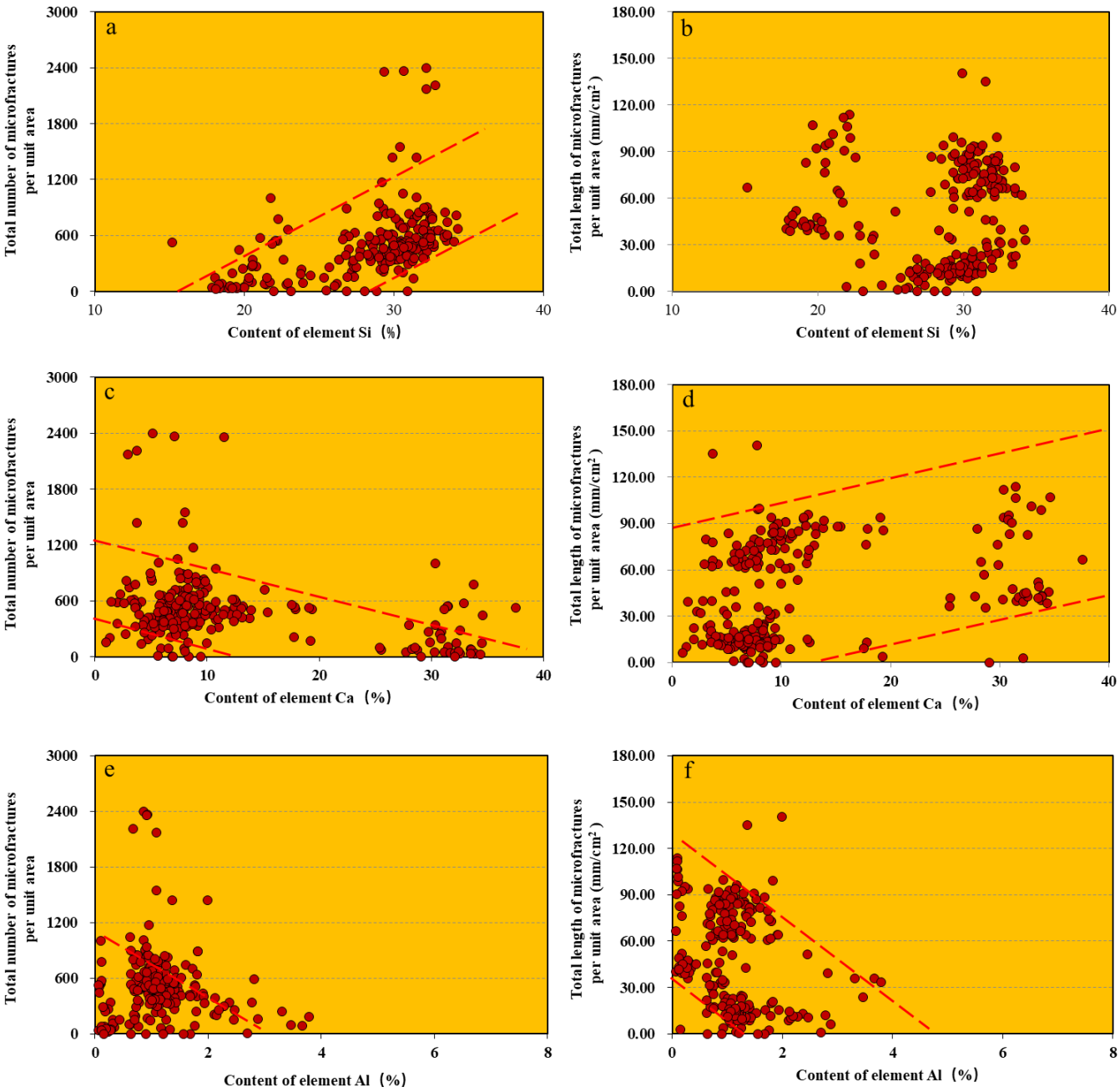

FIGURE 20: Relationship between Si, Ca, and Al element content and total length and number of microfractures.

the higher the Al content, the smaller the number and length of microfractures (Figures 20(e) and (f)). The Al element represents the content of clay minerals, indicating that high content of clay mineral is not conducive to microfracture forming.

5.1.3.3. Brittleness index. Fractures are closely related to the BI, which is generally calculated from Young's modulus and Poisson's ratio, the ratio of core samples can be determined using triaxial stress experiments [83]. In this study, the BI of the samples was calculated using EDS results, and the relationship between the BI and microfractures was discussed (Figures 21(a)–(c)). In general, the degree of microfracture development correlates with the brittleness index of the reservoir, and the samples are clearly divided into two parts: the lower samples of profile represent the aspect ratio of around three, and the upper samples represent the aspect ratio of less than two. The length and number of microfractures are positively correlated with the BI (Figures 22(a) and (b)). The BI calculated based on the EDS mineral component only considers the mineral component, not the grain structure and other characteristics. Therefore, the positive correlation shows an obvious trend, the larger the BI, the greater the number of microfractures and the larger the total length for the same type of rock sample. From the graph of the relationship between the

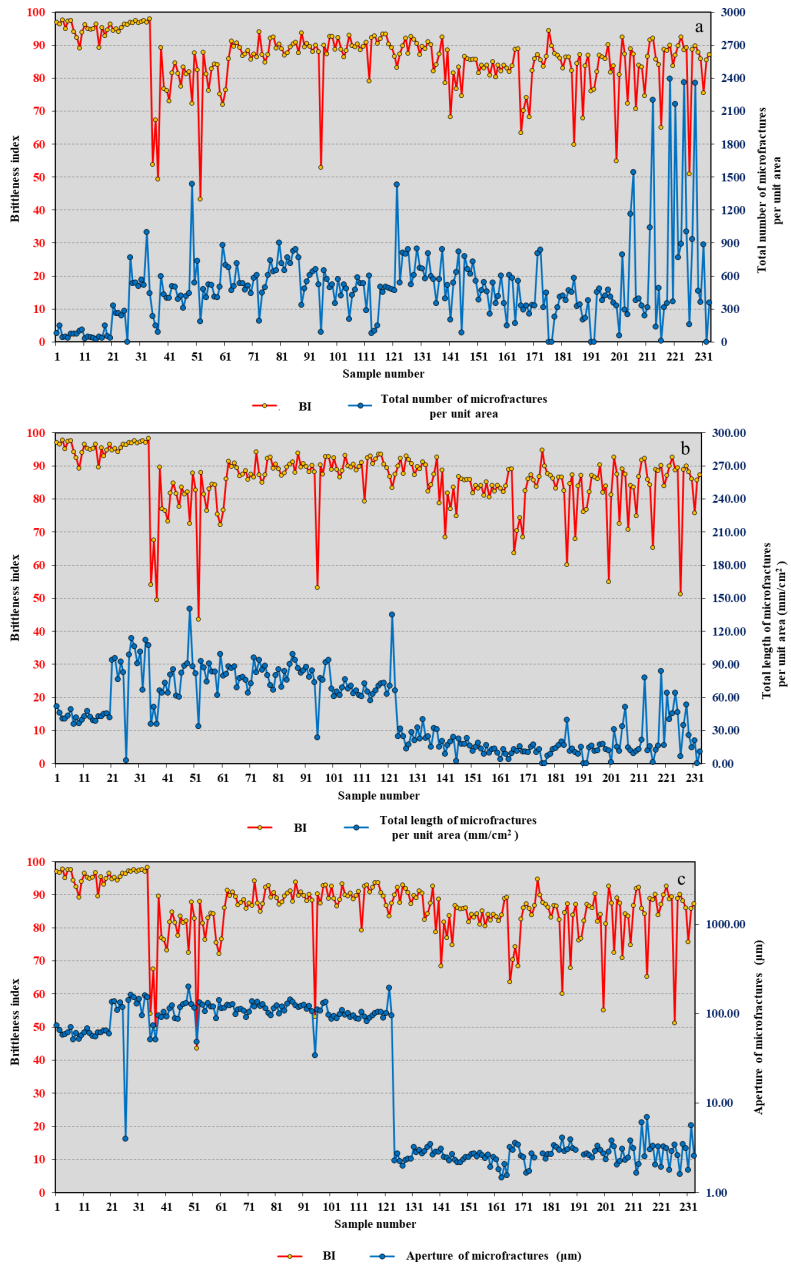

FIGURE 21: BI versus total number, total length, and aperture of microfractures. (a) Relationship between BI and total number of microfractures per unit area; (b) Relationship between BI and total length of microfractures per unit area; (c) Relationship between BI and microfacture aperture.

BI and the fracture aperture, a positive correlation can be observed between the BI and fracture aperture; the higher the BI, the larger the microfracture aperture (Figure 21(c)).

5.2. Multi-Scale Fracture Network and Production Capacity. Natural fractures of multi-scale form a fracture network. Large- and medium-scale tectonic fractures are large in scale and dominated by low- and medium-angle oblique intersections, whereas small-scale bedding fractures are small in lateral and vertical scales with limited distribution. Large- and medium-scale tectonic fractures are well-connected to high-quality reservoirs in different parts. Tectonic fractures and locally distributed bedding fractures are cut and connected to each other, forming a macroscopic fracture network in three-dimensional space. A large number of microfractures develop inside the tectonically fractured reservoirs, and intergranular microfractures are connected with the pore throat system, forming a multi-scale fracture network system.

The different types and scales of fractures make the fracture distribution in the Xinchang area complex. The complexity of the fractures is enhanced by multi-phase tectonic movements. The different scales of natural fractures effectively improved the reservoir storage and seepage capacity. The quantitative relationship between the fracture linear density of tectonic and bedding fractures,

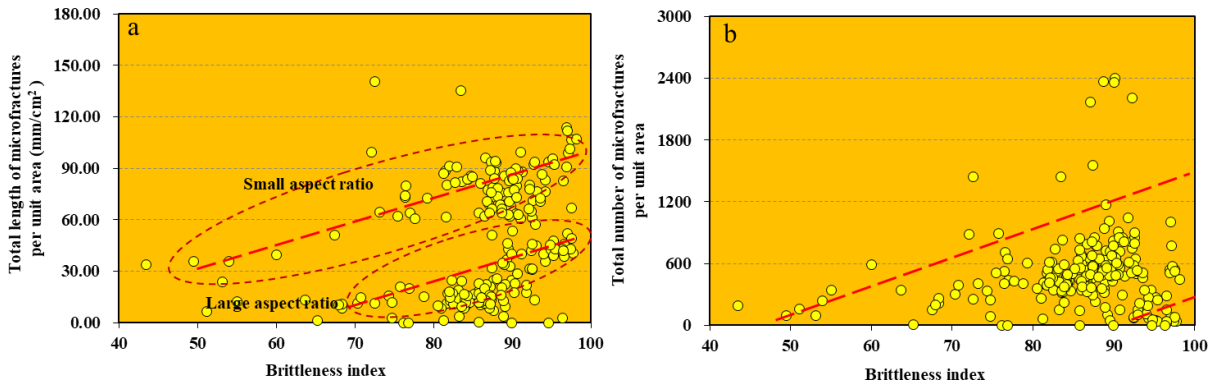

FIGURE 22: Relationship between the BI and total length and total number of microfractures.

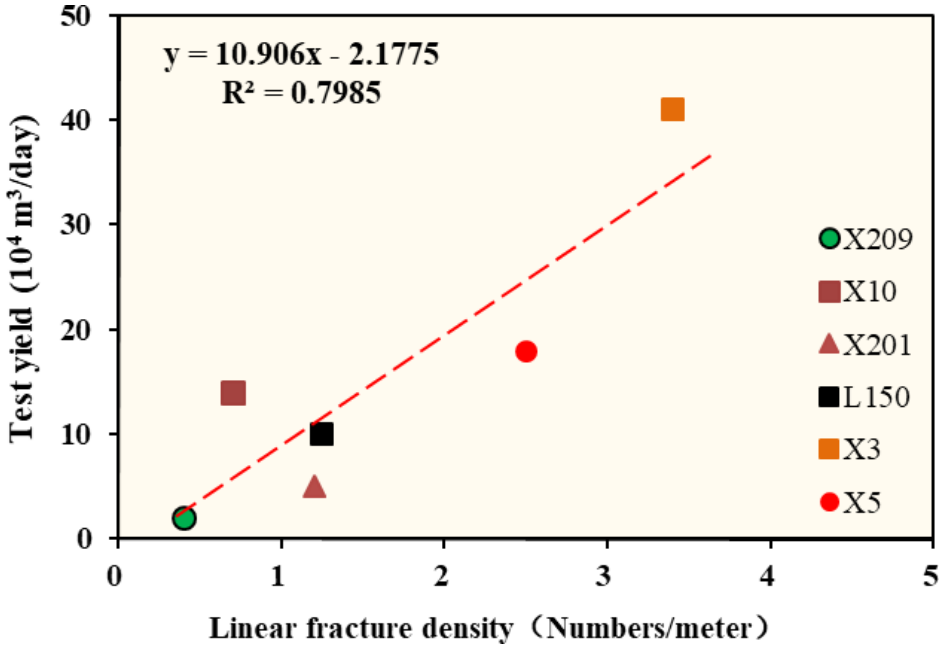

FIGURE 23: Relationship between fracture linear density and gas production in the second member of the Xinchang gas reservoir.

and the initial production capacity shows a substantial positive correlation (Figure 23). The microfractures improve the micro-seepage capacity. Multiscale fractures play a controlling role in the distribution of natural gas, which tends to accumulate along the fractures, and the multi-scale fractures have a greater impact on the initial gas production.

6. Conclusion

(1) The natural fractures in the second member of the Xinchang tectonic zone can be divided into three categories: tectonic, bedding, and microscopic fractures. The different types of fractures constitute the fracture network system. The tectonic fractures are mainly tensile fractures. The fracture occurrence is more in low- and medium-angles, mainly unfilled. The multiphase tectonic movements make the fractures show strong heterogeneity. The bedding fractures are nearly horizontally distributed with local intermittent or bifurcated features along the bedding surface, mostly unfilled. The bedding fractures are divided into parallel bedding, dark mineral interface, and carbonaceous fragment interface fractures, mainly formed by diagenesis, with a small lateral extension distance and a limited vertical distribution range. The microscopic fractures are quantitatively interpreted using a combination of scanning energy spectroscopy and electron microscopy. The microfractures in the study area mainly developed intra-grain, edge-grain, and inter-grain microfractures. Intragranular and edge-grain microfractures developed inside and at the edges of quartz or feldspar grains with small extension lengths, whereas intergranular microfractures ran through multiple grains, with longer extension lengths not limited by the grains and often with branching characteristics. Fractures of different scales can substantially increase the

reservoir permeability and improve seepage performance.

(2) The main factors controlling fractures in the second member of the Xujiahe Formation are discussed. The tectonic stress is an important factor, and the tectonic fractures are also closely related to lithology and stratum thickness. Lithology affects fractures through grain size, mineral components, argillaceous content, and so forth. There is a clear exponential relationship between the stratum thickness and the fracture linear density. The fracture linear density becomes larger in a certain range as the stratum thickness decreases. The bedding fractures in the second member are closely related to diagenesis. There are differences in the compaction and dissolution of different grain size and minerals in the diagenesis process, forming a mechanically weak surface and forming bedding fractures under the action of tectonic stress in the later stage. The parallel bedding fractures are controlled by the coupling of water depth and flow velocity. The bedding fractures at the interface of dark mineral and carbonaceous layers are controlled by the differences in rock components. The quartz and feldspar content of the dark mineral bedding fractures developed section is generally less than 75%, and the rock fragment content is generally more than 25%.

(3) The total length, number, and aperture of microfractures are controlled by the ratio of the long to short axes of grains. The grain aspect ratio is substantially negatively correlated with the total length and aperture of microfractures, which can be explained by the fact that the closer the ratio to 1, the closer the grain morphology to spherical shape, and the area of mutual contact between spherical grains is small, and the tectonic stress per unit area is larger, which is favorable to the development of microfractures. Microfracture development is also influenced by the content of particulate elements: Si, Ca, and Al. When the Si element content is higher, the total number of microfractures is higher; when the Ca element content is higher, the total length of the microfractures is larger, whereas the total number is not high. The Al content is negatively correlated with microfractures. The length and number of microfractures are positively correlated with the BI. The natural fractures have a great influence on the initial gas production, and natural fractures of different scales form a three-dimensional seepage system, which can effectively improve the seepage capacity of the reservoir.

Data Availability

Data will be made available on request.

Conflicts of Interest

The authors declare that they have no known competing financial interests or personal relationships that could have appeared to influence the work reported in the paper.

Acknowledgments

This study was supported by the National Natural Science Foundation of China (Grant No. 41902155 and 41502126). Special thanks are extended to anonymous reviewers for their critical and constructive reviews.

References

[1] R. Rezaee, A. Saeedi, and B. Clennell, "Tight gas sands permeability estimation from mercury injection capillary pressure and nuclear magnetic resonance data," *Journal of Petroleum Science and Engineering*, vols. 88–89, pp. 92–99, 2012.

[2] C. Zou, R. Zhu, K. Liu, et al., "Tight gas sandstone reservoirs in China: characteristics and recognition criteria," *Journal of Petroleum Science and Engineering*, vols. 88–89, pp. 82–91, 2012.

[3] S. Y. Hu, R. K. Zhu, S. T. Wu, B. Bai, Z. Yang, and J. W. Cui, "Profitable exploration and development of continental tight oil in China," *Petroleum Exploration and Development*, vol. 45, no. 4, pp. 790–802, 2018.

[4] A. L. Jia, Y. S. Wei, Z. Guo, G. T. Wang, D. W. Meng, and S. Q. Huang, "Development status and prospect of tight sandstone gas in China," *Natural Gas Industry B*, vol. 9, no. 5, pp. 467–476, 2022.

[5] C. Ma, C. Dong, C. Lin, et al., "Influencing factors and fracability of lacustrine shale oil reservoirs," *Marine and Petroleum Geology*, vol. 110, pp. 463–471, 2019.

[6] C. F. Ma, C. Y. Lin, C. M. Dong, et al, "Determination of the critical flow pore diameter of shale caprock," *Marine and Petroleum Geology*, vol. 112, p. 104042, 2020.

[7] B. Liu, J. Sun, Y. Zhang, et al., "Reservoir space and enrichment model of shale oil in the first member of Cretaceous Qingshankou Formation in the Changling sag, southern Songliao basin, NE China," *Petroleum Exploration and Development*, vol. 48, no. 3, pp. 608–624, 2021.

[8] B. Liu, Y. F. Gao, K. Q. Liu, et al., "Pore structure and adsorption hysteresis of the middle Jurassic Xishanyao shale formation in the Southern Junggar Basin, northwest China," *Energy Exploration & Exploitation*, vol. 39, no. 3, pp. 761–778, 2021.

[9] X. H. Ma, A. L. Jia, J. Tan, and D. B. He, "Tight sand gas development technologies and practices in China," *Petroleum Exploration and Development*, vol. 39, no. 5, pp. 611–618, 2012.

[10] J. Z. Li, B. C. Guo, M. Zheng, and T. Yang, "Main types, geological features and resource potential of tight sandstone gas in China," *Natural Gas Geoscience*, vol. 23, no. 4, pp. 607–615, 2012.

[11] J. X. Dai, Y. Y. Ni, and X. Q. Wu, "Tight gas in China and its significance in exploration and exploitation," *Petroleum Exploration and Development*, vol. 39, no. 3, pp. 277–284, 2012.

[12] J. Li, G. Q. Wei, Z. Y. Xie, R. E. Liu, and A. S. Hao, "Accumulation mechanism and main controlling factors of large tight sandstone gas fields in China:cases study on Ordos Basin and Sichuan Basin," Acta Petrologica Sinica, vol. 34, no. S1, pp. 14–28, 2013.

[13] D. B. He, A. L. Jia, G. Ji, Y. S. Wei, and H. F. Tang, "Well type and pattern optimization technology for large scale tight sand gas,sulige gas field," *Petroleum Exploration and Development*, vol. 40, no. 1, pp. 84–95, 2013.

[14] G. Q. Wei, F. D. Zhang, J. Li, et al., "New progress of tight sand gas accumulation theory and favorable exploration zones in China," *Natural Gas Geoscience*, vol. 27, no. 2, pp. 199–210, 2016.

[15] J. W. Zhao, H. M. Xu, C. He, et al., "Geological characteristics and main controlling factors of permian lacustrine tight oil in the eastern part of the Junggar Basin," *Geosciences Journal*, vol. 21, no. 2, pp. 187–200, 2017.

[16] J. W. Zhao and S. L. Yin, "Microscopic heterogeneity and distribution characteristics of reservoirs controlled by a sequence framework: a case study of the Donghe sandstone reservoir in the Tarim Basin, SW China," *Geological Journal*, vol. 56, no. 10, pp. 5343–5362, 2021.

[17] S. Y. Deng, T. R. Ye, Z. X. Lyv, and H. Zhang, "Characteristics of gas reservoirs in the 2nd member of the Xujiahe Formation in Xinchang structure in Western Sichuan," *Natural Gas Industry*, vol. 28, no. 2, pp. 42–45, 2008.

[18] S. Q. Zhang, "Discussion on development strategies Xu 2 gas reservoir in Xinchang in Western Sichuan Region," *Rsvr Eval & Dvlopmt*, 27–34, 2012.

[19] Z. P. Li, H. J. Ni, X. Ran, and G. B. Luo, "A deep investigation into tight clastic gas pooling mechanism and its application:A case study of the 2nd member of the Xujiahe Formation gas reservoirs in the Xinchang gas field, Sichuan basin," *Natural Gas Industry*, vol. 33(04, pp. 48–51, 2013.

[20] S. L. Yin, G. Y. Chen, L. Zhang, Y. C. Luo, C. P. Wang, and T. T. Liu, "The controlling effect of lithofacies architecture on high quality tight sandstone reservoirs: A case study of second member of the upper Triassic of Xujiahe Formation, Western Sichuan Depression,China," *Natural Gas Geoscience*, vol. 27, no. 7, pp. 1179–1189, 2016.

[21] H. R. Zheng, Z. Q. Liu, S. L. Xu, et al., "Progress and key research directions of tight gas exploration and development in Xujiahe Formation, Sinopec exploration areas, Sichuan Basin," *Oil & Gas Geology*, vol. 42, no. 4, pp. 765–783, 2021.

[22] R A Nelson, *Geological Analysis of Naturally Fractured Reservoirs*, Gulf Publishing Company, Texas, 1985.

[23] M. L. Cooke, J. A. Simo, C. A. Underwood, and P. Rijken, "Mechanical stratigraphic controls on fracture patterns within carbonates and implications for groundwater flow," *Sedimentary Geology*, vol. 184, nos. 3–4, pp. 225–239, 2006.

[24] J. G. Ramsay, "Development of chevron folds," *Geological Society of America Bulletin*, vol. 85, no. 11, 1974.

[25] J. Suppe, "Geometry and knematics of fault-bend folding," *American Journal of Science*, vol. 283, no. 7, pp. 684–721, 1983.

[26] J. Suppe, C. D. Connors, and Y. Zhang, "Shear fault-bend folding," *AAPG Mem*, 303–323, 2004.

[27] E. Finch, S. Hardy, and R. Gawthorpe, "Progressive rollover fault-propagation folding: A possible kinematic mechanism to generate regional-scale recumbent folds in shallow foreland belts," *AAPG Bulletin*, vol. 80, pp. 174–193, 1996.

[28] W. Jamison and A. Pope, "Geometry and evolution of a fault-bend fold: Mount Bertha anticline," *Geological Society of America Bulletin*, vol. 108, no. 2, pp. 208–224, 1996.

[29] E. Finch, S. Hardy, and R. Gawthorpe, "Discrete element modelling of contractional fault- propagation folding above rigid basement fault blocks," *Journal of Structural Geology*, vol. 25, no. 4, pp. 515–528, 2003.

[30] J. Tamara, A. Mora, W. Robles, et al., "Fractured reservoirs in the eastern Foothills, Colombia, and their relationship with fold kinematics," *AAPG Bulletin*, vol. 99, no. 8, pp. 1599–1633, 2015.

[31] H. Watkins, R. W. H. Butler, C. E. Bond, and D. Healy, "Influence of structural position on fracture networks in the Torridon Group, Achnashellach fold and thrust belt," *Journal of Structural Geology*, vol. 74, pp. 64–80, 2015.

[32] J. Lamarche, A. P. C. Lavenu, B. D. M. Gauthier, Y. Guglielmi, and O. Jayet, "Relationships between fracture patterns, geodynamics and mechanical stratigraphy in carbonates (South-East Basin, France)," *Tectonophysics*, vol. 581, pp. 231–245, 2012.

[33] E. Panza, F. Agosta, A. Rustichelli, et al., "Fracture stratigraphy and fluid flow properties of shallowwater, tight carbonates: the case study of the Murge Plateau (southern Italy)," *Marine and Petroleum Geology*, vol. 73, pp. 350–370, 2016.

[34] H. Watkins, C. E. Bond, A. J. Cawood, M. A. Cooper, and M. J. Warren, "Fracture distribution on the Swift Reservoir Anticline, Montana: Implications for structural and lithological controls on fracture intensity," *Geological Society, London, Special Publications*, vol. 487, no. 1, pp. 209–228, 2020.

[35] C. A. Underwood, M. L. Cooke, J. A. Simo, and M. A. Muldoon, "Stratigraphic controls on vertical fracture patterns in Silurian Dolomite, northeastern Wisconsin," American Association of Petroleum Geologists Bulletin, vol. 87, no. 1, pp. 121–142, 2003.

[36] Z. Lianbo and L. Xiang-Yang, "Fractures in sandstone reservoirs with ultra-low permeability: A case study of the upper triassic Yanchang Formation in the Ordos Basin, China," *AAPG Bulletin*, vol. 93, no. 4, pp. 461–477, 2009.

[37] R. N. McGinnis, D. A. Ferrill, A. P. Morris, K. J. Smart, and D. Lehrmann, "Mechanical stratigraphic controls on natural fracture spacing and penetration," *Journal of Structural Geology*, vol. 95, pp. 160–170, 2017.

[38] R. Dashti, H. Rahimpour-Bonab, and M. Zeinali, "Fracture and mechanical stratigraphy in naturally fractured carbonate reservoirs-a case study from Zagros region," *Marine and Petroleum Geology*, vol. 97, pp. 466–479, 2018.

[39] F. Balsamo, F. H. R. Bezerra, A. B. Klimchouk, et al., "Influence of fracture stratigraphy on hypogene cave development and fluid flow anisotropy in layered carbonates," *Marine and Petroleum Geology*, vol. 114, no. 104507, p. 104207, 2020.

[40] Q. D. Boersma, L. A. N. R. Douma, G. Bertotti, and A. Barnhoorn, "Mechanical controls on horizontal stresses and fracture behaviour in layered rocks: A numerical sensitivity analysis," *Journal of Structural Geology*, vol. 130, p. 103907, 2020.

[41] J. F. W. Gale and J. Holder, "Natural fractures in some US shales and their importance for gas production,"in *Geological*

Society, London, Petroleum Geology Conference Series, 7:pp. 1131–1140, 2010.

[42] W. T. Zeng, J. C. Zhang, W. L. Ding, et al., "Fracture development in Paleozoic shale of Chongqing area (south China). Part one: fracture characteristics and comparative analysis of main controlling factors," *Journal of Asian Earth Sciences*, vol. 75, pp. 251–266, 2013.

[43] L. B. Zeng, W. Y. Lyu, J. Li, et al., "Natural fractures and their influence on shale gas enrichment in Sichuan Basin, China," *Journal of Natural Gas Science and Engineering*, vol. 30, pp. 1–9, 2016.

[44] Y. Y. Zhang, Z. L. He, S. Jiang, et al., "Fracture types in the lower cambrian shale and their effect on shale gas accumulation, Upper Yangtze," *Marine and Petroleum Geology*, vol. 99, pp. 282–291, 2019.

[45] X. Zhang, W. Shi, Q. Hu, et al., "Developmental characteristics and controlling factors of natural fractures in the lower Paleozoic marine shales of the upper Yangtze Platform, southern China," *Journal of Natural Gas Science and Engineering*, vol. 76, p. 103191, 2020.

[46] Y. Gu, W. Ding, Q. Tian, et al., "Developmental characteristics and dominant factors of natural fractures in lower Silurian marine organic-rich shale reservoirs: A case study of the Longmaxi Formation in the Fenggang Block, southern China," *Journal of Petroleum Science and Engineering*, vol. 192, p. 107277, 2020.

[47] Z. J. Wu, H. J. Tang, and F. S. An, "Causese of bedding fractures of tight sand gas-reservoir in Xinchang, West Sichuan region," *Petrol Explor*, 109–111, 2003.

[48] L. B. Zeng, W. Y. Lyv, X. Xu, H. Tian, S. L. Lu, and M. J. Zhang, "Development characteristics,formation mechanism and hydrocarbon significance of bedding fractures in typical tight sandstone and shale," Acta Petrologica Sinica, vol. 43, no. 2, pp. 180–191, 2022.

[49] M. Mokhtari and A. N. Tutuncu, "Characterization of anisotropy in the permeability of organic-rich shales," *Journal of Petroleum Science and Engineering*, vol. 133, pp. 496–506, 2015.

[50] B. J. Cardott, C. R. Landis, and M. E. Curtis, "Post-oil solid Bitumen network in the Woodford Shale, USA—a potential primary migration pathway," *International Journal of Coal Geology*, vol. 139, pp. 106–113, 2015.

[51] A. Pluymakers, M. Kobchenko, and F. Renard, "How microfracture roughness can be used to distinguish between exhumed cracks and in-situ flow paths in Shales," *Journal of Structural Geology*, vol. 94, pp. 87–97, 2017.

[52] M. J. Blunt, "Flow in porous media—pore-network models and multiphase flow," *Current Opinion in Colloid & Interface Science*, vol. 6, no. 3, pp. 197–207, 2001.

[53] H. Dong and M. J. Blunt, "Pore-network extraction from micro-computerized tomography images," *Physical Review. E, Statistical, Nonlinear, and Soft Matter Physics*, vol. 80, no. 3 Pt 2, 2009.

[54] S. Williams-Stroud, C. Ozgen, and R. L. Billingsley, "Microseismicity-constrained discrete fracture network models for stimulated reservoir simulation," *Geophysics*, vol. 78, no. 1, pp. B37–B47, 2013.

[55] Y. Liang, "Rock fracture skeleton tracing by image processing and quantitative analysis by geometry features," *Journal of Geophysics and Engineering*, vol. 13, no. 3, pp. 273–284, 2016.

[56] S. Karimpouli, P. Tahmasebi, H. L. Ramandi, P. Mostaghimi, and M. Saadatfar, "Stochastic modeling of coal fracture network by direct use of micro-computed tomography images," *International Journal of Coal Geology*, vol. 179, pp. 153–163, 2017.

[57] J. C. Dick, A. Shakoor, and N. Wells, "A geological approach toward developing a mud rock-durability classification system," *Canadian Geotechnical Journal*, vol. 31, no. 1, pp. 17–27, 1994.

[58] A. Ougier-Simonin, F. Renard, C. Boehm, and S. Vidal-Gilbert, "Microfracturing and microporosity in shales," *Earth-Science Reviews*, vol. 162, pp. 198–226, 2016.

[59] H. Panahi, M. Kobchenko, P. Meakin, D. K. Dysthe, and F. Renard, "Fluid expulsion and microfracturing during the pyrolysis of an organic rich shale," *Fuel*, vol. 235, pp. 1–16, 2019.

[60] X. J. Wang, Z. R. Yang, and B. Han, "Superposed evolution of Sichuan Basin and its petroleum accumulation," *Earth Science Frontiers*, vol. 22, no. 3, pp. 161–173, 2015.

[61] Z. W. Li, S. G. Liu, J. Lin, C. Tang, B. Deng, and W. Sun, "Structural configuration and its genetic mechanism of the west Sichuan depression in China," *Journal of Chengdu University of Technology(Science & Technology Edition)*, vol. 36, no. 6, pp. 645–653, 2009.

[62] Z. Q. Liu, S. L. Xu, J. L. Liu, et al., "Enrichment laws of deep tight sandstone gas reservoirs in the Western Sichuan Depression, Sichuan Basin," *Natural Gas Industry*, vol. 40, no. 2, pp. 31–40, 2020.

[63] S. Liu, X. G. Ren, S. X. Yao, et al., "Relationship between gas reservoir distribution and structural system of Upper Triassic Xujiahe Fm in the Sichuan Basin," *Natural Gas Industry*, vol. 38, no. 11, pp. 1–14, 2018.

[64] K. M. Yang, J. Ye, and Z. X. Lyv, "Characteristics of gas distribution and reservoiring in Upper Triassic Xujiahe Formation in Western Sichuan Depression," *Oil & Gas Geology*, vol. 25, no. 5, pp. 501–505, 2004.

[65] T. R. Ye, S. B. Li, Z. X. Lyv, and G. M. Ke, "Sequence stratigraphic framework and sedimentary system distribution of the Xujiahe Formation in the Sichuan basin," *Natural Gas Industry*, vol. 31, no. 9, pp. 51–57, 2011.

[66] R. K. Zhu, B. Bai, L. H. Liu, L. Su, Z. Y. Gao, and Z. Luo, "Research on standardization of continental sequence stratigraphy and Palaeogeography: A case study from the Upper Triassic Xujiahe Formation in Sichuan Basin," *Earth ScienceFrontiers*, vol. 18, no. 4, pp. 131–143, 2011.

[67] R. C. Zheng, Z. C. Dai, R. K. Zhu, W. L. Zhai, H. C. Gao, and W. Geng, "Sequence-based lithofacies and paleogeographic characteristics of upper Triassic Xujiahe Formation in Sichuan Basin," *Geological Review*, vol. 55, pp. 484–495, 2009.

[68] Q. Hao, L. B. Lin, Y. Yu, S. H. Xu, and L. J. Qian, "Provenance analysis and main controlling factors of second member Xujiahe Formationin West Sichuan Depression," *Science Technology and Engineering*, vol. 14, no. 26, pp. 5–12, 2014.

[69] X. L. Wang, L. Liu, L. B. Lin, et al., "Sedimentary micro-facies and distribution of sand bodies in the 2nd member of Xujiahe Formation, Xinchang area, Western Sichuan Depression, China," *Journal of Chengdu University of Technology(Science & Technology Edition)*, vol. 48, no. 1, pp. 23–34, 2021.

[70] Y. L. Kang and P. Y. Luo, "Current status and prospect of key techniques for exploration and production of tight sandstone gas reservoirs in China," Petroleum Exploration and Development, vol. 34, no. 2, pp. 239–245, 2007.

[71] Q. Lei, Y. J. Wan, X. Z. Li, and Y. Hu, "A study on the development of tight gas reservoirs in the USA," *Natural Gas*, 2010.

[72] S. F. Wang, W. H. An, P. Chen, D. T. Liu, and H. J. Liang, "Characteristic and development techniques of Sulige tight gas pool," *Natural Gas Geoscience*, vol. 24, pp. 138–145, 2013.

[73] A. L. Jia, Y. S. Wei, Z. Guo, G. T. Wang, D. W. Meng, and S. Q. Huang, "Development status and prospect of tight sandstone gas in China," *Natural Gas Industry*, vol. 42, pp. 83–92, 2022.

[74] W. Y. Lyu, L. B. Zeng, J. Liu, C. Y. Wang, and J. Zhu, "Fracture research progress in low permeability tight reservoirs," Geological Science and Technology Information, vol. 35, no. 4, pp. 66–75, 2016.

[75] W. Y. Lyu, L. B. Zeng, S. B. Zhou, et al., "Natural fractures in tight-oil sandstones: a case study of the Upper Triassic Yanchang formation in the southwestern Ordos basin," *AAPG Bulletin*, vol. 103, no. 10, pp. 2343–2367, 2019.

[76] C. G. Liang, Q. Luo, J. F. Zhang, et al., "Analysis of Imbibition difference between bedding fractures and structural fractures in tight sandstore reservoir: a case study in Lucaogou formation in Jimsar depression," *Petroleum Geology and Recovery Efficiency*, vol. 27, no. 4, pp. 104–110, 2020.

[77] W. C. Wang, "Cross bedding types of sedimentary rocks and their environmental significance," *Minerals and Rocks*, vol. 5, no. 4, pp. 63–70, 1985.

[78] D. Z. Dong, Z. S. Shi, S. S. Sun, et al., "Factors controlling microfractures in black shale: a case study of Ordovician Wufeng Formation-Silurian Longmaxi Formation in Shuanghe profile, Changning area, Sichuan basin, SW China," *Petroleum Exploration and Development*, vol. 45, no. 5, pp. 818–829, 2018.

[79] Z. Y. Gao, X. B. Yang, C. H. Hu, et al., "Characterizing the pore structure of low permeability Eocene Liushagang formation reservoir rocks from Beibuwan Basin in northern south China sea," *Marine and Petroleum Geology*, vol. 99, pp. 107–121, 2019.

[80] L. B. Zeng, P. Lyv, X. F. Qu, and J. M. Fan, "Multi-scale fractures in tight sandstone reservoirs with low permeability and geological conditions of their development," *Oil & Gas Geology*, vol. 41, no. 3, pp. 449–454, 2020.

[81] R. A. Nelson, E. P. Moldovanyi, C. C. Matcek, I. Azpiritxaga, and E. Bueno, "Production characteristics of the fractured reservoirs of the la paz field maracaibo basin, Venezuela," American Association of Petroleum Geologists Bulletin, vol. 84, no. 11, pp. 1791–1809, 2000.

[82] K. Ogata, F. Storti, F. Balsamo, et al., "Sedimentary facies control on mechanical and fracture stratigraphy in turbidites," *Geological Society of America Bulletin*, vol. 129, nos. 1–2, pp. 76–92, 2017.

[83] S. Wang, B. Liu, X. F. Fu, and W. C. Zhao, "Evaluation of the brittleness and fracturing characteristics for tight clastic reservoir," *Oil & Gas Geology*, vol. 39, no. 6, pp. 1270–1279, 2018.